Palaeogeography, Palaeoclimatology, Palaeoecology 423 (2015) 18–31

Contents lists available at ScienceDirect

Palaeogeography, Palaeoclimatology, Palaeoecology

journal homepage: www.elsevier.com/locate/palaeo

Recurrent phases of drought in the upper Miocene of the Black Sea region

Iuliana Vasiliev [a,b,*], Gert-Jan Reichart [a,c], Arjen Grothe [d], Jaap S. Sinninghe Damsté [a,c], Wout Krijgsman [b], Francesca Sangiorgi [d], Johan W.H. Weijers [a], Linda van Roij [a]

[a] Organic Geochemistry, Department of Earth Sciences, Utrecht University, Budapestlaan 4, 3584 CD Utrecht, The Netherlands
[b] Paleomagnetic Laboratory 'Fort Hoofddijk', Department of Earth Sciences, Utrecht University, Budapestlaan 17, 3584 CD Utrecht, The Netherlands
[c] Royal Netherlands Institute of Sea Research, P.O. Box 59, 1790 AB Den Burg, Texel, The Netherlands
[d] Marine Palynology and Paleoceanography, Laboratory of Palaeobotany and Palynology, Department of Earth Sciences, Utrecht University, Budapestlaan 4, 3584 CD Utrecht, The Netherlands

ARTICLE INFO

Article history:
Received 28 October 2014
Received in revised form 18 January 2015
Accepted 21 January 2015
Available online 31 January 2015

Keywords:
Black Sea
Miocene
Hydrogen isotopes
Carbon isotopes
Alkenones
n-Alkanes
TEX_{86}
SSTs
Palynology

ABSTRACT

Since the Miocene the Black Sea proved to be highly sensitive to fluctuations in the hydrological cycle because of its recurrent restricted connections with the open ocean and the location between the dry Mediterranean and more humid higher northern latitudes. Although the Black Sea formed one of the foci of the 1975 Deep Sea Drilling Project Leg 42B, robust tools to reconstruct past changes in its hydrological cycle were lacking at that time. Here we revisit the sedimentary succession (Hole 380A) and determined compound-specific carbon ($\delta^{13}C$) hydrogen isotope ratios (δD) of terrestrial and aquatic biomarkers to investigate changes in the hydrological budget of the Black Sea during the late Miocene. The $\delta^{13}C$ and δD isotopic composition of *n*-alkanes as well as alkenones and palynology indicate large environmental changes in the Black Sea and/or in the sources of the water entering the Black Sea during the late Miocene. The δD of alkenones, showing an enrichment of more than 80‰ at the end of the Miocene, implies a major shift in basin hydrology, possibly resulting in severely increased salinity. These changes in δD composition of the alkenones coincide with both with sharp shifts in reconstructed sea surface temperature and palynological assemblages. Two intervals with negative water budget were identified, most likely caused by enhanced evaporation. The older and longer dry/evaporative phase predates the Maeotian/Pontian boundary (regional stages) at ~6.1 Ma. The younger drying phase corresponds to the Messinian Salinity Crisis. This shift to highly evaporative conditions is related to a similar shift previously observed in a Messinian (Pontian) sedimentary succession from the Taman Peninsula (Russia). These recurrent dry phases likely reflect regional climatic shifts over a significantly larger area around the Black Sea area during the upper Miocene.

1. Introduction

Landlocked marine basins like the Black Sea, the Red Sea and the Mediterranean are highly sensitive to changes in their hydrological cycles. Modifications in river runoff, evaporation and precipitation are quickly reflected in salinity and circulation changes. In general, a freshwater deficit results in an anti-estuarine circulation (e.g., present-day Mediterranean Sea, Red Sea), whereas a freshwater surplus leads to stratification and ultimately outflow of surface waters (e.g., present-day Black Sea, Baltic Sea). The water balance of these basins is delicate and critically depends on connections to the ocean or to other subbasins, which are known to have changed frequently over geological past. During the latest Miocene, the Mediterranean suffered from a major restriction event, the so-called Messinian Salinity Crisis (MSC, 5.97–5.33 Ma) (Hsü et al., 1973; Krijgsman et al, 1999; Manzi et al., 2013) when a severe deficit in the water budget of the Mediterranean interrupted the already limited water exchange with both the Atlantic and the Black Sea (e.g., Roveri et al., 2014).

To reconstruct the Messinian imprint of hydrological changes on the Black Sea, we recently analyzed changes in compound-specific hydrogen isotope compositions (δD) of molecular biomarkers in sedimentary successions of the Taman Peninsula (Russia) (Vasiliev et al, 2013). These data showed a shift towards much enriched δD values in the Black Sea occurring at the time when the Mediterranean suffered severe restrictions of the connection to the Atlantic Ocean during the MSC. These severely enriched δD data can be explained by two scenarios: 1) the Black Sea had a negative hydrological budget when it became isolated from the Mediterranean during the peak MSC event (~5.6 Ma) or 2) the Black Sea basin was affected by an influx of δD heavy waters sourced from the highly evaporative Mediterranean. This reconstruction could potentially be biased by the marginal setting of Taman (Vasiliev et al, 2013). Therefore, the present study aims for a confirmation of this event in the deeper part of the Black Sea basin.

Here we reconstruct hydrological and environmental changes in the deep Black Sea basin using excellently preserved biomarkers extracted from cores of Deep Sea Drilling Project (DSDP) Leg 42B Hole 380A

* Corresponding author at: Paleomagnetic Laboratory 'Fort Hoofddijk', Department of Earth Sciences, Utrecht University, Budapestlaan 17, 3584 CD, Utrecht, The Netherlands.
E-mail addresses: i.vasiliev@uu.nl, iuli.iuliana@yahoo.com (I. Vasiliev).

http://dx.doi.org/10.1016/j.palaeo.2015.01.020
0031-0182/

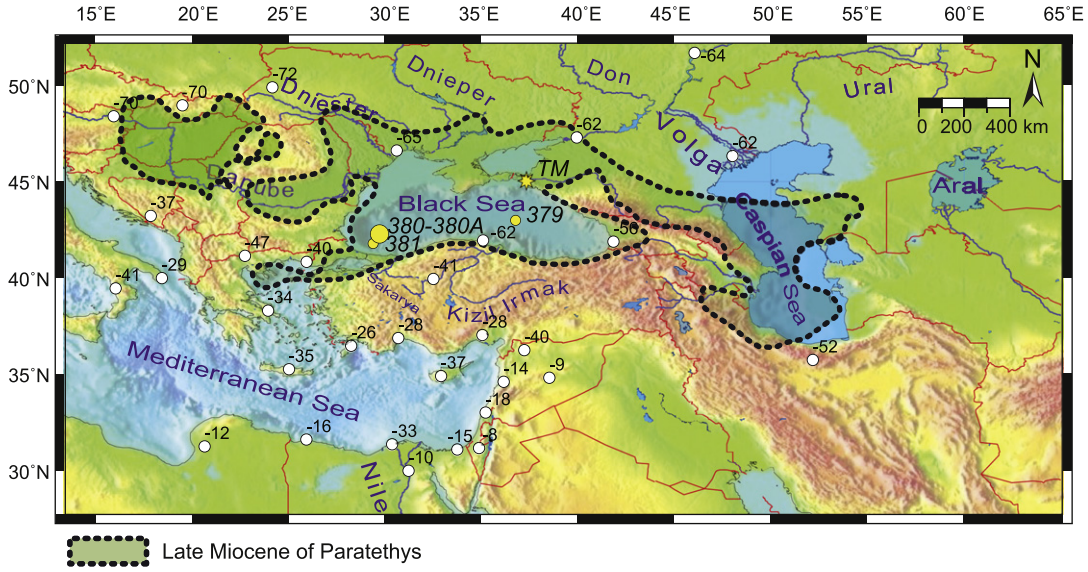

Fig. 1. Paleogeographic map of the late Miocene, showing the Paratethys area on the presented day land configuration. Major rivers draining into the Paratethys – former sea of Eurasia – (Rögl, 1999) are indicated (modified after Vasiliev et al., 2013). The values of the present day precipitation δD are reported according to IAEA (2001). Long-term means were calculated by selecting yearly means in which isotope content have been measured at least in 75% of the precipitation for that year and at least over eight months (IAEA, 2001). Deep Sea Drilling Project 42B Holes 379, 380 and 381 are indicated. The star locates the Taman Peninsula (TM) with Zheleznyi Rog section used in Vasiliev et al. (2013).

(Fig. 1). Although these cores have been drilled almost 40 years ago, recent insights in the Black Sea stratigraphy and advancements in the stable isotopic composition of organic components allows unraveling the fundamental changes in climate and basin geometry in controlling the hydrology of the Black Sea in the past. Long chain *n*-alkanes are terrestrial biomarkers derived from higher plant waxes, and their hydrogen isotopic composition is used to reconstruct hydrological changes on continental realm surrounding the Black Sea. In contrast, the hydrogen isotopic record of long-chain alkenones produced by haptophyte algae reflects changes in the composition of Black Sea water. Additionally, sea surface temperatures (TEX_{86} proxy) and palynological data provide independent assessments of changes in the Black Sea hydrology. With this study we aim 1) to investigate whether the hydrological changes during the MSC observed in the Taman Peninsula record represent a basin wide event and 2) to extend the organic geochemical record further back in time.

2. Stratigraphy of sampled interval

The cores of DSDP Leg 42B Hole 380A (42° 05.94′ latitude and 29° 36.82′ longitude) were drilled in 1975 north of the Bosporus (Fig. 1) and represent a more than 1000 m thick sedimentary record of the Black Sea covering a time interval from the late Miocene to the Quaternary. Hole 380A was drilled at the foot of the continental slope at 2115 m water depth. We analyzed the lower part of this set of cores, from 1072.5 to 738 meters below sea floor (mbsf) (Fig. 2). The sampled interval covers five lithological (sub)units as defined in the initial reports (Ross and Neprochnov, 1978): unit V consisting of black shale (1072.5–969 mbsf); unit IVe of 'carbonate' (969–883.5 mbsf); unit IVd of pebbly mudstone (883.5–864.5 mbsf); unit IVc of aragonitic mud (864.5–850.3 mbsf) and part of unit IVb, the so-called 'seekreide' (850.3–718 mbsf) (Fig. 2).

The chronostratigraphy of Hole 380A has remained controversial ever since its recovery from the sea floor (Fig. 2). In particular, the age of an alleged desiccation event suggested by the pebbly mudstone (unit IVd) remained controversial. Hsü and Giovanoli (1979) interpreted this unit as being late Messinian in age, assuming that the Black Sea level was drawn down nearly to the abyssal plain as a consequence of the MSC. In this scenario, the overlying unit of aragonitic mud (unit IVc) would mark the early Pliocene flooding (5.33 Ma) (Fig. 2a). In contrast, Kojumdgieva (1979, 1983) interpreted the pebbly mudstone unit to mark deep desiccation of the Black Sea during the late Khersonian (Paratethys regional stage; ~8–9 Ma), while the aragonitic mud unit

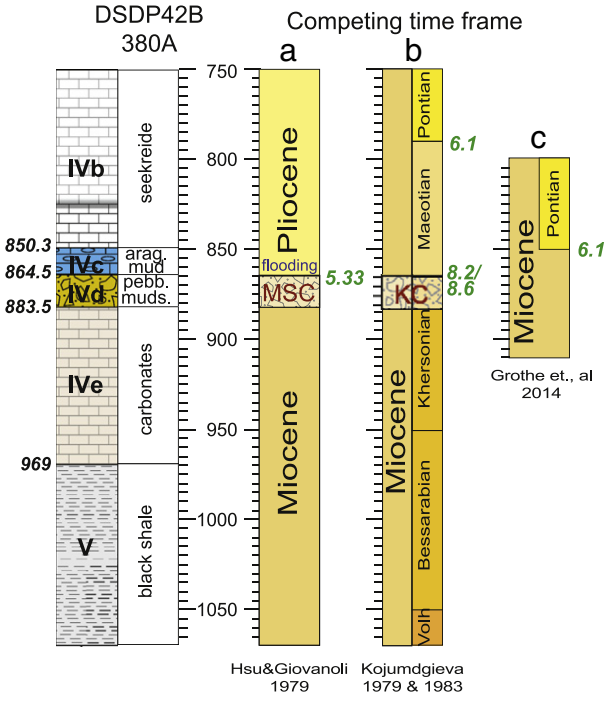

Fig. 2. Competing time frames for the DSDP 42B Hole 380A. a) In Hsü and Giovanoli (1979) the Miocene–Pliocene boundary corresponds to the IVd/IVc transition, between 'pebbly mudstone' and 'aragonitic mud'. The interpreted Messinian Salinity Crisis (MSC) interval is represented. b) In Kojumdgieva's (1979, 1983) interpretation the IVd/IVc transition, between 'pebbly mudstone' and 'aragonitic mud' indicates Khersonian/Maeotian transition, marking a Khersonian crisis (KC). Volhinian, Bessarabian and Khersonian are sub-stages of Sarmatian s.l. of Eastern Paratethys. Sarmatian–Maeotian boundary age according to Vasiliev et al. (2011) and Maeotian–Pontian boundary age according to Krijgsman et al., 2010. c) New constraints on dinocyst assemblages indicate the top of 'aragonitic mud' unit (IVc) as starting at ~6.1 Ma (Grothe et al., 2014). The schematic lithology as defined in the initial reports is presented in the left hand side. In addition, an extra level (at 826.65 mbsf) is represented, marking obvious transition towards much darker level.

was linked to the onset of marine sedimentation during the regional Maeotian Stage (Fig. 2b). Recently, Hole 380A was correlated to the biomagnetostratigraphically dated Taman section using dinoflagellate cysts, which indicated that the pebbly mudstone unit (IVd) is older than the paleomagnetic reversal from C3An.1n to C3r (at 6.033 Ma) (Grothe et al., 2014) and thus predates the onset of the MSC in the Mediterranean Basin at 5.97 Ma (Fig. 2c) (Manzi et al., 2013).

3. Experimental methods

3.1. Lipid extraction, separation and analyses

Fifty six sedimentary rock samples weighing between 8 and 60 g were dried and thoroughly ground. To avoid possible contamination, which may have occurred during drilling and core handling, the outer part of the cores was avoided during sampling. Larger samples (i.e., 15–60 g), were extracted using a Soxhlet apparatus with a DCM–methanol (7.5:1, v/v) mixture. Smaller samples (up to 15 g) were extracted by accelerated solvent extraction (ASE, Dionex 200) using a dichloromethane (DCM)–methanol (9:1, v/v) organic solvent mixture at 100 °C and 1000 psi. All extracts were rotary-evaporated to near dryness and subsequently further dried under a nitrogen flow. The total lipid extracts (TLE) were dried over an anhydrous Na_2SO_4 column. Elemental sulfur was removed using activated copper in DCM. Copper flakes were activated with 2 M HCl and afterwards rinsed with MilliQ ultra-pure water, methanol and DCM. This treatment was repeated up to three times when necessary. An aliquot of the extract was separated using column chromatography with activated Al_2O_3 as stationary phase by subsequent elution with *n*-hexane/DCM (9:1, v/v), *n*-hexane/DCM (1:1, v/v), and a mixture of DCM/methanol (1:1, v/v) to obtain the apolar, ketone and polar fraction, respectively. *n*-Alkanes were isolated from the apolar fraction using urea-adduction. To this end, the apolar fraction was dissolved in 200 μl methanol/urea (~10%, H_2NCONH_2, Merck) solution. Subsequently, 200 μl acetone and 200 μl *n*-hexane were added to the solution, frozen (−20 °C) and dried under N_2 flow. Urea crystals were washed with *n*-hexane to remove the non-adductable branched and cyclic compounds and subsequently dissolved in 500 μl methanol and 500 μl MilliQ ultra-pure water mixture. The *n*-alkanes were extracted from the solution using *n*-hexane. The urea-adduction procedure was repeated up to three times to eliminate non-adductable compounds as much as possible. Alkenones were obtained from the ketone fraction using urea adduction as well using the same procedure. The *n*-alkanes and alkenones were identified based on mass spectra using gas chromatography–mass spectrometry (GC–MS) on a Thermo-Finnigan Trace DSQ instrument. The fractions (dissolved in *n*-hexane) were injected on-column at 70 °C (CP-Sil 5CB fused silica column; 30 m × 0.31 mm i.d.; film thickness 0.1 μm). The oven was set at constant pressure (100 kPa) and then programmed to increase to 130 °C at 20 °C min^{-1}, and then at 5 °C min^{-1} to 320 °C at which it was held isothermal for 10 min.

3.2. Compound-specific hydrogen isotope analyses

Compound-specific hydrogen isotope (δD) values of *n*-alkanes and alkenones were determined by gas chromatography–isotope ratio mass spectrometry (GS–IRMS). δD compositions of individual *n*-alkanes and alkenones were measured on the adducted *n*-alkane and alkenone fractions on a HP 6890 N gas chromatograph (GC) coupled to a Thermo-Finnigan Delta Plus XP Isotope Ratio Mass Spectrometer (IRMS). The fractions (dissolved in hexane) were injected on-column at 70 °C, the oven being programmed to increase to 130 °C at 20 °C min^{-1}, and then at 5 °C min^{-1} to 320 °C at which it was held isothermal for 10 min. The film thickness of the CP-Sil 5 column was 0.4 μm and a constant flow of He was used at 1.5 ml min^{-1}. Eluting compounds were on-line pyrolyzed in an empty ceramic tube heated at 1450 °C, which was pre-activated by a 5 min methane flow of 0.5 ml min^{-1}. H_3+ factors were determined daily on the isotope ratio mass spectrometer and were at any time <5. H_2 gas with known isotopic composition was used as reference and a mixture of C_{16}–C_{32} *n*-alkanes with known isotopic composition (ranging from −42‰ to −256‰ vs. Vienna Standard Mean Ocean Water (V-SMOW)) was used to monitor the performance of the system (Schimmelman Mixtures A and B, Biogeochemical Laboratories, Indiana University). A squalane standard was co-injected with every sample and its average value was −171 ± 3‰, which compared favorably with its offline determined value of −168.9‰. Each fraction was measured between two and ten times.

3.3. Compound-specific carbon isotope analyses

The carbon isotope ratios ($\delta^{13}C$) of individual *n*-alkanes and alkenones were measured on the adducted apolar and alkenone fractions on the GC–IRMS using similar conditions as for δD measurements. The $\delta^{13}C$ values, expressed relative to the V-PDB standard, were calculated by comparison to a CO_2 reference gas (calibrated against NBS-19). Standards deviations were determined using a co-injected standard and are ±0.3‰.

3.4. HPLC/MS analysis

The polar fraction was concentrated under a gentle N_2 stream, dissolved in *n*-hexane:2-isopropanol (99:1, v/v) and filtered over a 0.4 μm PTFE filter prior to injection into an high performance liquid chromatography–atmospheric pressure chemical ionization/mass spectrometry (HPLC–MS) as described by Hopmans et al. (2000). Analyses were performed using an Agilent 1290 Infinity series, 6130 Quadrupole UHPLC/MS equipped with auto-injector and Chemstation chromatography manager software. 10 μl of each polar fraction was injected and separation was achieved on an analytical Alltech Prevail Cyano column by elution with 90% *n*-hexane and 10% 9:1 (v/v) *n*-hexane:2-propanol, isocratically for the first 5 min (flow rate 0.2 ml min^{-1}) followed by a linear gradient to 18% 9:1 (v/v) *n*-hexane:2-propanol in 45 min. After each analysis, the column was cleaned by back-flushing *n*-hexane:2-propanol (9:1; v/v). Detection was achieved using positive ion APCI of the eluent. Conditions for the Agilent 1290 series were as follows: drying gas flow was set to 6.0 l min^{-1} with a temperature of 200 °C, a nebulizer pressure of 25 psi, a vaporizer temperature of 400 °C, a capillary voltage of −3.5 kV and a corona current of 5 μA. Isoprenoidal and branched glycerol dialkyl glycerol tetraether (GDGT) lipids were detected by scanning for their $[M + H]^+$ ion in selected ion monitoring (SIM) mode and quantified against a known amount of a C_{46} GDGT internal standard with an assumed relative response factor of 1, i.e., equal ionization efficiency for the different compounds (Huguet et al., 2006). We analyzed both isoprenoid and branched GDGT within a single acquisition run for each sample (Fig. 3). Fractional abundances of each isoprenoid and branched GDGT component were obtained by normalizing each peak area to the summed area of all isoprenoid and branched GDGTs.

3.5. Sea surface temperature calculation

Over the last ten years a novel organic sea surface water temperature proxy was increasingly applied based on the relative abundance of GDGT lipids, the TEX_{86} (TetraEther indeX of tetraethers consisting of 86 carbon atoms) proxy (Schouten et al., 2002; Kim et al., 2008). TEX_{86} values were calculated according to the definition of Schouten et al. (2002) as follows:

$$TEX_{86} = \frac{[GDGT\text{-}1] + [GDGT\text{-}2] + [Cren']}{[GDGT\text{-}0] + [GDGT\text{-}1] + [GDGT\text{-}2] + [Cren']}$$

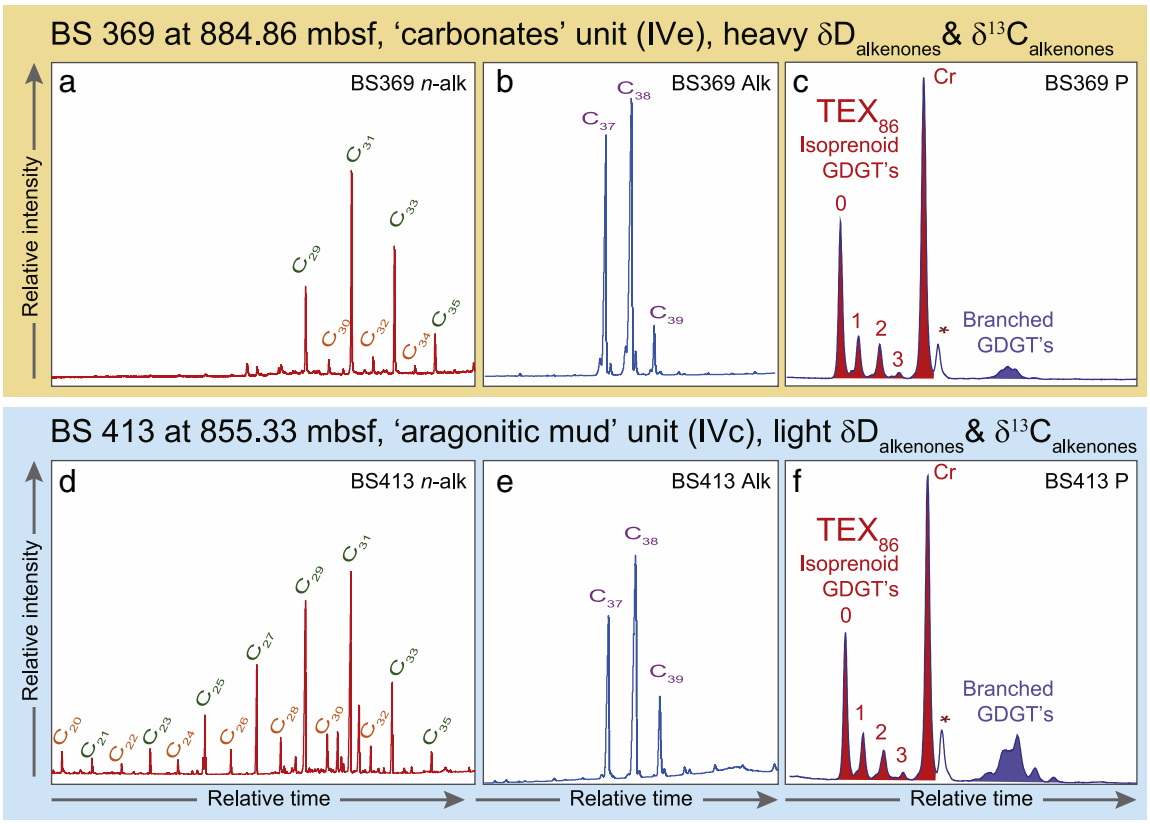

Fig. 3. Representative chromatograms of biomarker fractions of two representative sedimentary samples of the DSDP 42B 380A core. The presented examples are BS 369 at 884.68 meters below sea floor (mbsf) from 'carbonates' (IVe) unit (upper panels) and BS 413 at 855.33 mbsf from 'aragonitic mud' (IVc) unit (lower panels). a) and d) The adduct of the apolar fraction; note the *n*-alkanes with a distinctly odd (green) over even (orange) carbon-number predominance. Note the higher contribution of shorter chain *n*-alkanes in sample BS 413. b) and e) The alkenones fraction. Note the similarity of the alkenone distribution in both sediments although they belong to levels with the distinctly different $\delta D_{alkenone}$. c) and f) HPLC–MS base peak chromatograms of GDGTs showing the dominance of isoprenoidal (0, 1, 2, 3) vs. branched (III, II, I, Ib, Ic) GDGTs. Cr indicates crenarchaeol while * denotes the standard. Note the higher contribution of branched GDGTs in the sample BS 413P.

where *GDGT*-0, *GDGT*-1, *GDGT*-2 and *Cren′* are isoprenoid GDGTs with the structures presented in Supplementary Fig. 1. TEX_{86} values were transformed into sea surface temperature (SST) using the calibration of Kim et al. (2008) where $T = -10.78 + 56.2 \times TEX_{86}$. However, the application of TEX_{86} is limited to sedimentary archives where the terrestrial soil organic matter input is low (Weijers et al., 2006). The relative input of soil organic matter in marine sediments can be assessed using the branched and isoprenoid tetraether (BIT) index (Hopmans et al., 2004), calculated as:

$$BIT = \frac{[I + II + III]}{[I + II + III] + [Cren']}$$

where *I*, *II* and *III* are branched GDGTs with the structures presented in Supplementary Fig. 1.

3.6. Palynological analysis

In total, twenty samples were processed following standard palynological techniques used at the Laboratory of Palaeobotany and Palynology (LPP) of Utrecht University described in Brinkhuis et al. (2003). In short, 1–4 g of dried sediment was spiked with a known amount of *Lycopodium* spores, and treated with 30% HCl and 38% HF for carbonate and silicate removal, respectively. Residues were sieved using a 10-μm nylon mesh. Palynomorphs (pollen, spores, dinoflagellate cysts, the green freshwater algae *Pediastrum*, and acritarchs) were analyzed and counted at 400× or 1000× magnification. The percentage of aquatic palynomorphs (dinocysts, arcitarchs and *Pediastrum*) was calculated on a sum of aquatic and terrestrial palynomorphs (pollen excluding Bisaccates and spores). The relative abundance of the selected aquatic taxa presented is based on the total aquatic palynomorphs.

4. Results

4.1. n-Alkane abundance

The apolar fractions contain a series of *n*-alkanes ranging from *n*-C_{18} to *n*-C_{35}, with the long-chain (C_{27}–C_{31}) *n*-alkanes having the highest abundances. These long-chain *n*-alkanes show a strong odd-over-even carbon number predominance (Fig. 3a and d). At some intervals the contribution of the shorter chain *n*-alkanes is somewhat higher (Fig. 3d) although the long-chain (C_{27}–C_{31}) *n*-alkanes clearly dominate the distribution (Fig. 3a and d).

4.1.1. n-Alkane δD ratios

The δD of the C_{29} and C_{31} *n*-alkanes range between −170‰ and −210‰ (Table 1) and co-vary showing a moderate correlation (R^2 = 0.57; Fig. 4a). In general, the δD values of the C_{29} *n*-alkane are somewhat less negative than those of the C_{31} *n*-alkane (Fig. 4a and Table 1). From 875 mbsf towards the younger part of the sampled interval the $\delta D_{n\text{-alkanes}}$ show increasing variability (Fig. 5).

4.1.2. n-Alkane $\delta^{13}C$ values

The stable carbon isotopic composition of the C_{29} and C_{31} *n*-alkanes ($\delta^{13}C_{n\text{-alkanes}}$) varies between −27‰ to −35‰ (Table 1) and co-vary showing a moderate correlation (R^2 = 0.63; Fig. 4b). The $\delta^{13}C$ values of the C_{29} *n*-alkane are most of the time slightly less negative than those of the C_{31} *n*-alkane (Table 1). Up to 858 mbsf, the $\delta^{13}C$ values of

Table 1
δD isotopes measured on DSDP 42B 380A core. The δD_{precip} is calculated for a 'wet' climate using Sachse et al. (2006) and for a 'dry' climate using Feakins and Sessions (2010). Average, standard deviation (STDEV) and standard error of the means (SEM) are listed; n.d. denotes levels where the $\delta^{13}C$ or δD were not determined.

Sample code	Level (mbsf)	$\delta D_{nC_{29}}$ (‰)	N	SEM	$\delta D_{nC_{31}}$ (‰)	N	SEM	δDpp from $\delta D_{nC_{29}}$ (‰)		δDpp from $\delta D_{nC_{31}}$ (‰)		$\delta C_{nC_{29}}$ (‰)	N	SEM	$\delta C_{nC_{31}}$ (‰)	N	SEM
								Wet	Dry	Wet	Dry						
BS 292	1074.34	n.d.			n.d.			n.d.	n.d.	n.d.	n.d.	−30.4	1		−31.5	1	
BS 297	1064.22	−177.5	3	1.9	−176.3	3	0.7	−55	−96	−53	−95	−29.4	1		−29.9	1	
BS 299	1054.65	−173.5	2	6.5	−175.3	4	5.5	−50	−91	−52	−93	n.d.			n.d.		
BS 301	1047.5	−187.9	3	0.8	−184.0	3	1.1	−67	−108	−62	−103	−30.0	2	0.0	−30.7	2	0.0
BS 302	1040.65	−185.9	3	6.6	−183.7	3	4.4	−64	−106	−62	−103	−30.8	3	0.4	−32.1	2	0.4
BS 303	1040.27	−187.1	3	5.0	−185.5	3	5.8	−66	−107	−64	−105	n.d.			n.d.		
BS 305	1027.65	−187.4	2	5.8	−185.4	2	4.0	−66	−107	−64	−105	−30.7	1		−32.0	1	
BS 308	1020.82	−182.5	3	4.5	−181.3	4	2.7	−60	−102	−59	−100	−30.8	1		−32.1	1	
BS 315	1008.13	−177.2	4	6.0	−182.5	4	3.8	−54	−96	−60	−102	−31.1	1		−32.1	1	
BS 319	983.05	−172.4	1		−178.9	1		−49	−90	−56	−98	n.d.			n.d.		
BS 321	980.05	−172.0	2	1.7	−176.0	2	0.2	−48	−90	−53	−94	−30.8	3	0.1	−31.9	3	0.3
BS 324	974.05	−181.7	1		−169.6	1		−59	−101	−46	−87	n.d.			n.d.		
BS 326	970.65	−175.1	4	1.4	−177.8	4	0.9	−52	−93	−55	−96	−30.2	2	0.0	−31.5	2	0.1
BS 328	951.5	−169.7	1		−170.6	1		−46	−87	−47	−88	−29.9	1		−30.8	1	
BS 331	940.53	−182.0	2	2.1	−178.8	2	5.1	−60	−101	−56	−97	−29.6	2	0.4	−31.9	2	0.3
BS 333	932.7	−179.2	5	2.5	−184.7	5	2.8	−57	−98	−63	−104	n.d.			n.d.		
BS 335	933.74	n.d.			−189.1	1		n.d.	n.d.	−68	−109	−29.4	2	0.4	−30.0	2	0.1
BS 336	929.26	−170.1	5	2.1	−175.0	5	0.9	−46	−87	−52	−93	−30.2	2	0.1	−31.2	2	0.0
BS 339	924.2	−171.0	2	5.1	−175.5	2	4.4	−47	−89	−52	−94	−30.6	2	0.2	−31.6	2	0.2
BS 338	923.08	−175.4	4	0.9	−184.2	4	0.8	−52	−94	−62	−104	n.d.			n.d.		
BS 358	917.62	−170.9	2	1.3	−177.1	2	3.8	−47	−88	−54	−96	n.d.			−30.3	1	
BS 362	905.4	−180.4	1		−181.6	1		−58	−99	−59	−101	n.d.			n.d.		
BS 361	904.22	−170.2	4	1.7	−177.6	4	1.7	−46	−88	−55	−96	−31.2	5	0.3	−31.7	6	0.3
BS 364	886.63	−184.0	2	4.8	−191.2	2	2.4	−62	−103	−70	−112	−29.7	1		−29.3	1	
BS 367	886.3	−172.1	3	4.3	−177.9	3	1.8	−48	−90	−55	−96	n.d.			n.d.		
BS 369	884.68	n.d.			n.d.			n.d.	n.d.	n.d.	n.d.	−26.6	1		−28.9	1	
BS 368	883.92	−186.5	1		−180.6	1		−65	−106	−58	−100	−29.2	4	0.5	−30.9	4	0.4
BS 401	867.62	−192.7	1		−193.5	1		−72	−113	−73	−114	−29.3	3	0.3	−30.9	3	0.3
BS 408	861.4	−178.3	1		−193.1	2	4.5	−56	−97	−73	−114	−30.4	1		−30.8	1	
BS 410	858.63	−172.9	1		n.d.			−49	−91	n.d.	n.d.	−28.0	3	0.4	−27.2	3	1.1
BS 412	856.98	−174.5	3	1.5	−188.5	4	4.8	−51	−93	−67	−109	−29.5	2	0.8	−30.8	2	0.4
BS 413	855.33	−190.2	2	1.1	−195.4	3	5.3	−69	−111	−75	−117	−31.2	4	0.3	−32.2	4	0.5
BS 415	850.16	n.d.			−187.0	1		n.d.	n.d.	−65	−107	n.d.			n.d.		
BS 416	850.9	−186.8	2	1.4	−192.5	2	0.0	−65	−107	−72	−113	−31.5	3	0.9	−32.7	3	0.2
BS 417	848.5	−184.7	2	2.5	−197.7	2	2.0	−63	−104	−78	−119	−30.3	4	0.6	−30.3	4	0.5
BS 419	845.67	−169.3	2	1.0	−177.1	2	1.0	−45	−87	−54	−96	−30.9	2	2.3	−32.0	2	1.1
BS 422	841.26	−166.1	2	5.9	−172.1	2	5.3	−41	−83	−48	−90	−31.2	2	0.3	−31.9	2	0.4
BS 421	840.5	−178.1	3	4.5	−177.8	3	4.4	−55	−97	−55	−96	−31.4	1		−33.2	1	
BS 424	839.8	n.d.			−210.8	1		n.d.	n.d.	−93	−134	n.d.			n.d.		
BS 423	839.11	−177.8	2	1.3	−171.0	2	0.9	−55	−96	−47	−88	−30.7	1		−31.5	1	
BS 426	836.86	−182.2	1		−199.8	1		−60	−101	−80	−122	−30.0	1		−30.1	1	
BS 425	836.11	−183.4	2	0.8	−191.7	4	7.6	−61	−103	−71	−112	n.d.			n.d.		
BS 428	829.2	−189.6	2	3.2	−197.1	3	2.6	−69	−110	−77	−118	−31.4	1		−31.1	1	
BS 430	826.9	−185.8	1		−192.0	1		−64	−106	−71	−113	−32.7	1		−32.7	1	
BS 434	825.8	−195.8	3	4.4	−189.5	1		−76	−117	−68	−110	−32.2	2	0.3	−32.1	2	0.5
BS 437	820.75	−178.4	2	4.6	−175.8	2	4.5	−56	−97	−53	−94	−31.1	1		−33.0	1	
BS 445	800.18	−178.2	1		−190.6	2	7.5	−55	−97	−70	−111	n.d.			n.d.		
BS 447	792.1	−168.8	3	5.3	−175.5	3	0.7	−45	−86	−52	−94	−30.3	2	0.0	−31.5	2	0.6
BS 451	779.65	−173.0	2	5.5	−176.3	2	3.3	−49	−91	−53	−95	−31.7	2	0.4	−33.8	2	0.4
BS 457	774.71	−209.2	1		−209.0	1		−91	−132	−91	−132	n.d.			n.d.		
BS 462	757.67	−179.6	1		n.d.			−57	−98	n.d.	n.d.	n.d.			n.d.		
BS 463	752.16	−200.6	3	2.4	−193.1	3	3.5	−81	−123	−73	−114	−31.7	2	0.3	−35.2	2	0.7

n-alkanes are more or less stable at ca. −31‰ for the C_{29} *n*-alkane (Table 1 and Fig. 5) and ca. −32‰ for the C_{31} *n*-alkane (Table 1). From 858 mbsf towards the top of the sampled interval the $\delta^{13}C_{n\text{-alkanes}}$ show a trend towards more negative values of about −35‰ (C_{31}) near the top of the studied interval (Table 1).

4.2. Long-chain ketones

The ketone fractions show the presence of long-chain unsaturated ethyl and methyl ketones (alkenones) (C_{37}–C_{39}) (Fig. 3b and e). Alkenones were detected from a depth of 930 mbsf to the top of the sampled interval (Figs. 5 and 6). The alkenone distribution shows a remarkable dominance of the C_{38} ketone and appreciable concentrations of the C_{39} ketone. Both C_{37} and C_{38} ketones are dominated by the di-unsaturated components.

4.2.1. Alkenone δD values

The stable hydrogen isotopic composition of the C_{37} and C_{38} alkenones ($\delta D_{alkenone}$) varies markedly between −224‰ and −140‰ (‰ V-SMOW) (Table 2) and show a strong correlation ($R^2 = 0.84$; Fig. 4c). Throughout the record, the δD values of the C_{37} and C_{38} alkenones closely track each other, albeit with a small offset (Table 2). The base of the record shows values between −140‰ and −180‰. A sudden shift towards more negative $\delta D_{alkenone}$ values of −224‰ occurs in the middle of the aragonitic unit IVc, at 858 mbsf. Values increase again at 827 mbsf, coinciding with a peculiar dark layer. In the younger

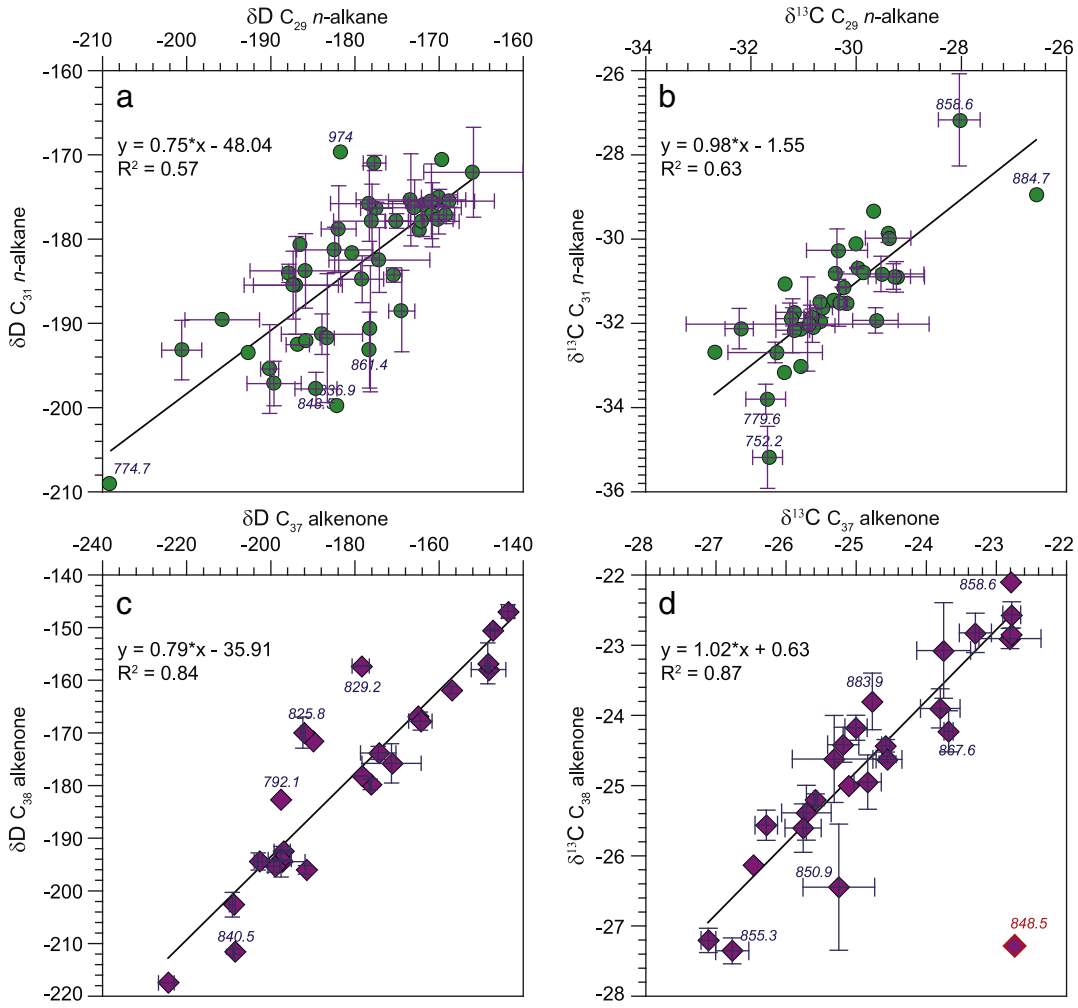

Fig. 4. Cross plots of $\delta^{13}C$ and δD measured on *n*-alkanes and long chain alkenones from DSDP 42B Hole 380A. The numbers in italics indicate stratigraphic levels (in mbsf) of samples further from the correlation lines. a) Comparison of measured $\delta^{13}C$ on C_{29} and $\delta^{13}C$ on C_{31} *n*-alkanes; b) Comparison of measured δD on C_{29} and δD on C_{31} *n*-alkanes; c) Comparison of measured $\delta^{13}C$ on C_{37} and $\delta^{13}C$ C_{38}; d) Comparison of measured δD on C_{37} and δD on C_{38} alkenones. The sample at 848.5 mbsf is considered an outlier and not taken into consideration for the presented linear correlation.

strata values shift towards about −200‰, staying more or less stable towards the top (Table 2 and Figs. 5 and 6).

4.2.2. Alkenone $\delta^{13}C$ values

The stable carbon isotopic compositions of the C_{37} and C_{38} alkenones ($\delta^{13}C_{alkenones}$) vary between −21‰ to −27‰ (Table 1) showing a strong correlation ($R^2 = 0.87$; Fig. 4d). The $\delta^{13}C$ values of the C_{37} and C_{38} alkenones closely correspond, showing the same trend through time (Table 1 and Fig. 4d). However, the variation in $\delta^{13}C$ of the C_{37} alkenones within the investigated interval is 4.4‰, while that for the C_{38} alkenones is slightly larger, about 6‰ (Table 1). For clarity we present in Figs. 5 and 6 only the $\delta^{13}C$ of C_{37}. The $\delta^{13}C$ values of C_{37} alkenones are more or less constant around −23.5‰ until 858 mbsf within the 'aragonitic mud' (IVc), when an abrupt shift occurs towards values around −27.4‰ (Figs. 5 and 6). At 850.3 mbsf, marking the transition between the 'aragonitic mud' (IVc) and the 'seekreide' (IVb), the lightest value is observed (−27.4‰). The $\delta^{13}C_{alkenones}$ fluctuate around these light values until 840 mbsf, when they become more enriched again, subsequently staying stable at around −25‰. The record presented here ends with the heaviest value registered by C_{38} alkenones, at 750 mbsf (Table 2).

4.3. GDGT lipids

In all studied sediments both isoprenoid and branched GDGTs are well represented (Fig. 3c and f). For six out of the 48 samples analyzed, the calculated BIT index was >0.3. For calculating SSTs using TEX_{86} only samples with BIT index of <0.3 should be considered reliable (Weijers et al., 2006). Kim et al. (2008) proposes two calibrations for two different settings: 1) the one at 0 m water depth and 2) the one between 0 and 200 m water depth (Fig. 6). In our upper Miocene Black Sea record the SST estimates at 0 m water depth are between 3 and 6 °C higher than the estimates valid for water depths between 0 and 200 m. However, either calibration shows the same general trends, characterized by several sharp fluctuations (Fig. 6). We consider the usage of calibration between 0 and 200 m water depth to be more appropriate for the SST estimates in this Black Sea record because it will average the signal of the GDGTs deposited over a longer period of time and from the entire water column. Therefore, even if we already calculated both water depth situations and we plot both values in Fig. 6, we will expose in the following lines only the SST estimates using the calibration between 0 and 200 m water depth. With this provision, the SST record is characterized by a temperature change of 12 °C change. Between the base of the core and 930 mbsf, estimated temperatures are around 10 °C. Between 930 and ~887 mbsf a gradual shift occurs towards values of about 15 °C. The following 30 m of core, until 850.3 mbsf, shows a sharp ~6 °C decrease in SST. These low temperatures only continue for a short interval, after which a sharp increase of ~11 °C is observed at 835 mbsf to values of 20 °C. This sharp increase corresponds to transition between IVc and IVb, at 850 mbsf. A second temperature minimum

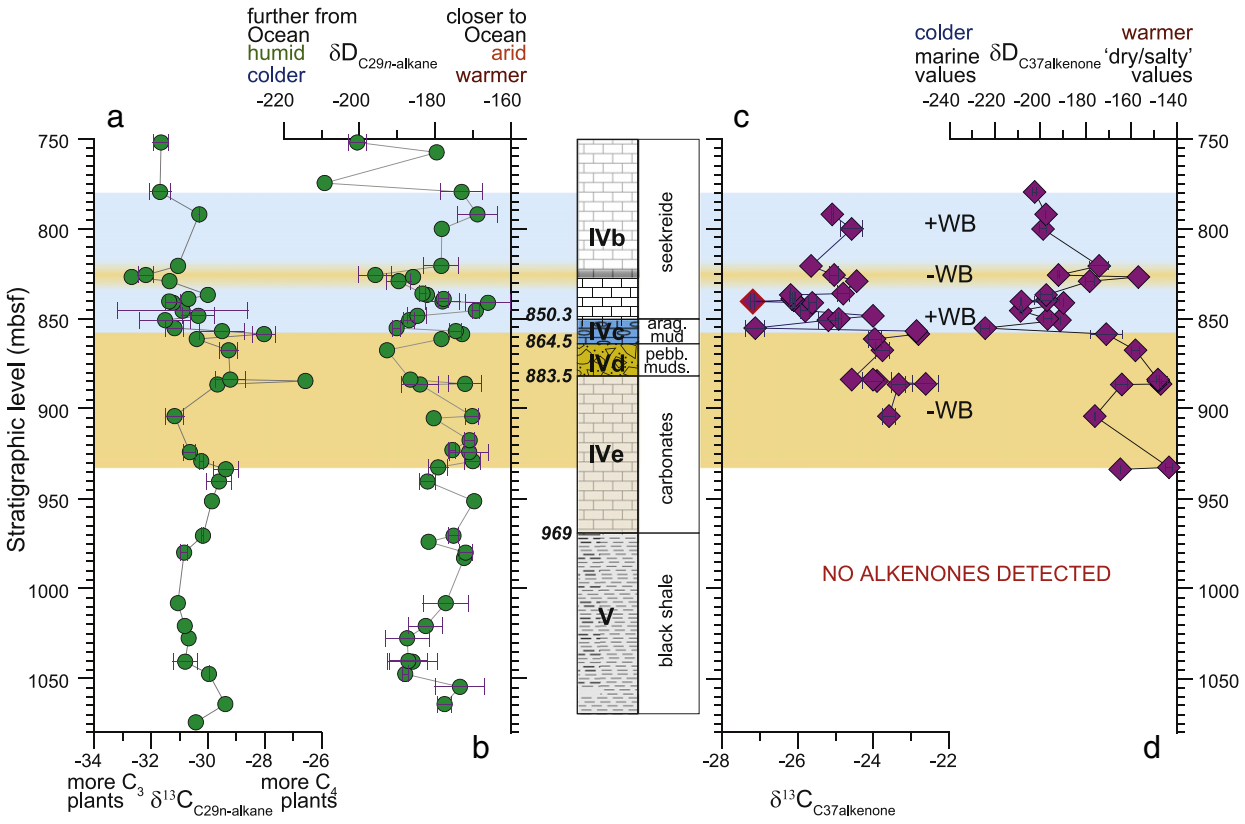

Fig. 5. $\delta^{13}C$ and δD isotopes of C_{29} *n*-alkane and C_{37} long chain alkenones. Schematic lithological column of the sedimentary succession at Hole 380A is presented between the *n*-alkane and alkenone records. The levels of lithological transitions, in mbsf, are in bold italics. The important variations in δD isotope values and implicitly of the hydrological balance are marked on the figure. Error bars are based on the standard deviation of the complete set of replicate analyses and indicate standard errors of the mean. Additionally, next to the δD scales are the indicated possible causes for lighter vs. heavier values recorded.

is observed at 830 mbsf after which temperature increases to 20 °C (Fig. 6).

4.4. Palynology

The aquatic/terrestrial percentages and the changes in the relative abundance of the most indicative aquatic palynomorphs (dinoflagellate cysts and acritarchs, *Pediastrum*) for environmental reconstructions are presented in Fig. 6. In general, the percentage of aquatic palynomorphs is generally low during the lower part of the record (units V–IVd), and become very low in unit IVe. The percentages of aquatic palynomorphs increase in the aragonitic mud (subunit IVc) and remain high within the 'seekreide' (IVb) (Fig. 6). The transition between units V and IV (~1000 and 950 mbsf) is marked by relatively higher abundances of aquatic palynomorphs. Among the dinoflagellate cysts, *Spiniferites* spp. (total taxa belonging to the genus *Spiniferites*, excluding *Spiniferites cruciformis*) is present throughout the record, being relatively more abundant in the lower part (units V and IVe). The dinocyst *Lingulodinium machaerophorum* peaks at 850.16 mbsf and is regularly present in the upper part of the record. The first consistent occurrence (FCO) of the Paratethyan endemic taxa (*Caspidinium rugosum*, *Galeacysta etrusca* and *S. cruciformis*) is encountered at the base of subunit IVb at 850.16 mbsf (Grothe et al., 2014). These taxa are constantly present in the upper part of the record. *Pyxidinopsis psilata* represents an important part of the palynological assemblage above ~836 mbsf. *Micrhystridium* shows two appreciable peaks, at the top of subunit IVd (pebbly mudstone) and in the lower part of the 'seekreide' (subunit IVb), respectively. The freshwater algae *Pediastrum*, which constitutes an important part of the palynological assemblages at the top of the units V and IVe, is hardly encountered above ~900 m.

5. Discussion

5.1. n-Alkanes and their δD and $\delta^{13}C$ isotopic compositions

In our record from the DSDP 42 B 380A Hole, the *n*-alkane fraction indicates a dominance of the long chain *n*-alkanes with an odd over even carbon-number predominance (Fig. 3a), indicative for major contribution of the higher plants (Eglinton and Hamilton, 1967). This observation is in line with the organic geochemistry results from the initial reports (Ross and Neprochnov, 1978). However, at some levels the contribution of the shorter chain *n*-alkanes is somewhat higher (Fig. 3e) indicating that some other (e.g., aquatic) plant groups contribute to the total *n*-alkane fraction.

5.1.1. n-Alkane δD values

δD ratios of *n*-alkanes have been shown to reflect primarily the δD composition of precipitation (e.g., Sachse et al., 2004a,b) and are affected, to a variable degree, by evapotranspiration (e.g., Sachse et al., 2006; Polissar and Freeman, 2010). Keeping in mind the plant-physiology-induced limitations to the quantitative interpretation of the δD_{water}, the $\delta D_{n\text{-alkanes}}$ have been successfully used in reconstruction of terrestrial paleo-$\delta D_{precipitation}$ and paleo-evaporation (e.g., Andersen et al., 2001; Sachse et al., 2004a; Schefuss et al., 2005; Pagani et al., 2006; Speelman et al., 2010; Tipple and Pagani, 2010; Feakins et al., 2013).

There is more than 35‰ amplitude in the $\delta D_{n\text{-alkane}}$ record of Hole 380A (Table 2 and Fig. 4a). This large variation hints to some important changes occurring in the hydrology or/and in the vegetation composition. To estimate the δD_{precip} we applied a constant biosynthetic fractionation between source water and *n*-alkane of 157‰ (Sessions et al., 1999; Sachse et al., 2006). Additionally, a different evapo-transpiration enrichment effect was applied for δD_{precip} calculations (Fig. 6;

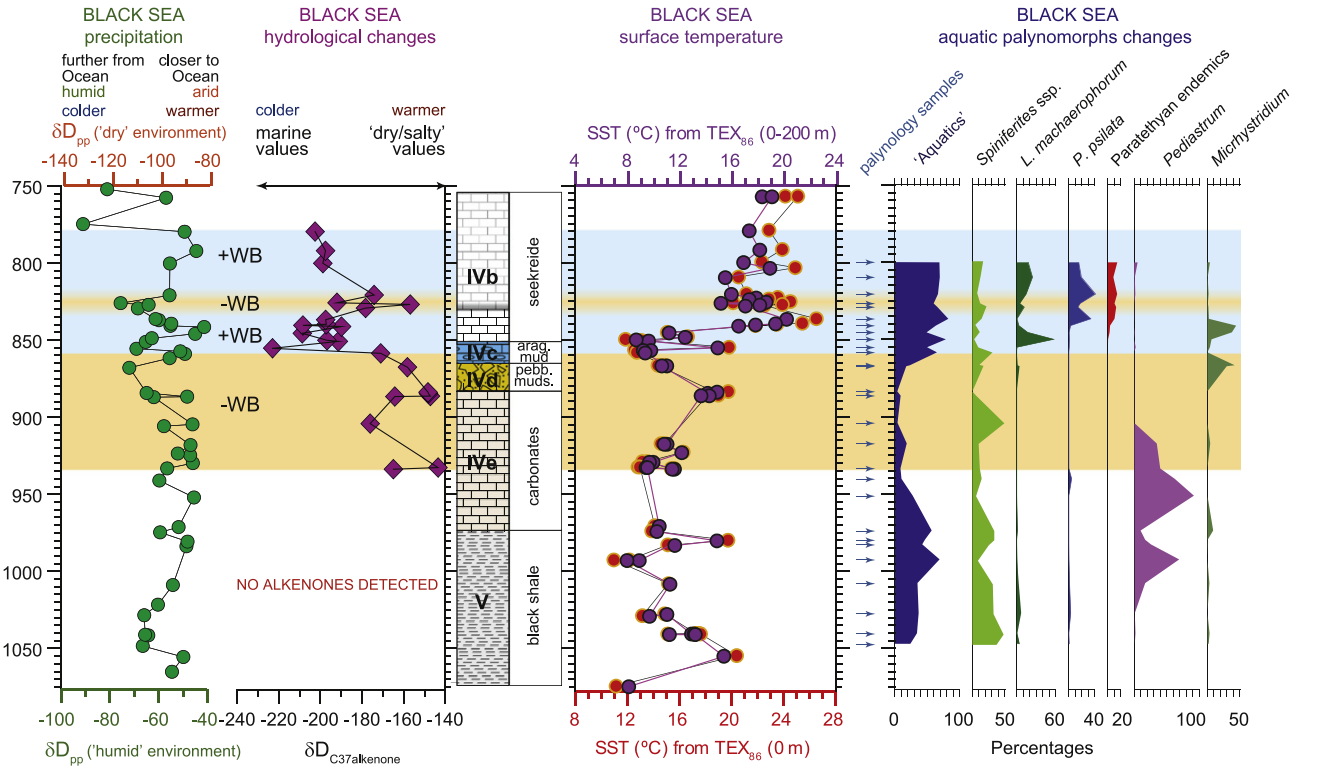

Fig. 6. Results summarizing δD measured on long chain alkenones and *n*-alkanes, SSTs estimates and palynology of DSDP 42B Hole 380A. In the central part of the figure the schematic lithological column of the sedimentary succession at Hole 380A is presented. The levels of lithological transitions, in mbsf, are in bold italics. The levels where marked switches in δD isotopes and implicitly hydrological balance take place are marked on the figure. These represent the level where different evapotranspiration effect could be used. Error bars are based on the standard deviation of the complete set of replicate analyses and indicate standard errors of the mean. Additionally, next to the δD scales are the indicated possible causes for lighter vs. heavier values recorded. On the left side δD precipitation values are calculated from $\delta D_{n\text{-}C29}$ *n*-alkanes for two scenarios 1) in the case of the European 'humid' temperate climate using the relation of Sachse et al. (2006) and 2) in the case of 'arid' climate using the relation of Feakins and Sessions (2010). Different scales are indicated for dry (at top) and humid (at base) climate effect on evapotranspiration. δD values for C_{37} alkenones are represented and used as primary indicators for switches in hydrological balance (marked on the figure with different shading). Different evapotranspiration in the calculation of δD_{pp} effect should be used at levels with marked switches in the hydrological balance. In the left hand side of the lithological column are plotted the SSTs estimates. The SST was calculates using two calibrations: 1) for 0 m depth in the lower axis of the graphic and 2) for 0–200 m depth in the top axis of the graphic. The most important palynological changes are plotted on the right hand side of this figure. Arrows indicate the levels which were analyzed for palynology The aquatic–terrestrial marine percentage ratio, here plotted as percentage aquatics, was calculated by taking the sum of the aquatic palynomorphs (dinocysts, arcitarchs and green algae) divided by the sum of the total palynomorphs including all aquatic and terrestrial palynomorphs except bisaccate pollen. The relative abundance of species or groups within the 'aquatics' using the sum of a certain species or group divided by the total sum of the aquatic palynomorphs. See Section 5.4 for paleoenvironmental interpretations.

Table 2): (1) of ~30‰ (Sachse et al., 2006) found in the modern Western Europe humid conditions and (2) of ~60‰ as described for arid ecosystem (Feakins and Sessions, 2010). Assuming a Western Europe like humid environment the δD_{precip} values would have varied between −93‰ and −46‰ (Fig. 6 and Table 2). These values largely overlap to δD_{precip} of around −62‰ recorded in the present day at stations north of the Black Sea (IAEA, 2001). In the case of prevailing arid conditions (possibly corresponding to intervals with heavy $\delta D_{alkenones}$) the calculated δD_{precip} would have varied between −134‰ and −87‰, typical values exclusively observed in cold northern high latitudes in Eurasia (IAEA, 2001). The heavier δD_{precip} towards the younger part of the record can be explained by three different mechanisms, or a combination thereof. First, a change in the dominant water vapor source could offset overall values. Second, distance to the vapor source might have decreased. Third, continental temperatures might have increased. All three proposed mechanisms would strongly influence the composition of the higher-plant vegetation which is the major producer of the long-chain *n*-alkanes and indirectly, alter the recorded $\delta D_{n\text{-}alkane}$ values.

5.1.2. n-Alkane $\delta^{13}C$ values

In contrast to hydrogen isotopes, stable carbon isotopic compositions of plant waxes reflect primarily different vegetation types. Leaf waxes from C_3 plants (95% of plant species on Earth, e.g., all trees) have a $\delta^{13}C$ as low as −35‰, whereas those from C_4 plants (e.g., grasses, savannah, salt marsh and desert plants) are as high as −21.7‰ (e.g., Castañeda and Schouten, 2011).

In the DSDP 42B Hole 380A, the largest amplitude in $\delta^{13}C_{n\text{-}alkane}$ values (C_{29} and C_{31}), switching from as heavy as −28‰ to −33‰ coincides with the level where the largest variation in $\delta D_{n\text{-}alkane}$ values appears, over a short interval at IVc/IVb transition (Fig. 5). Therefore, this decreasing trend of the $\delta^{13}C_{n\text{-}alkanes}$ starting at ~858 mbsf could be explained by an increase of C_3 versus C_4 plants contribution in the total vegetation. The vegetation composition is important because the discrimination against deuterium during photosynthesis is greater in C_3 plants (−117‰ to −121‰) than in C_4 plants (−86‰ to −109‰). A change in the evapo-transpiration enrichment effect could be considered for the samples younger than the 858 mbsf level. The $\delta^{13}C_{n\text{-}alkanes}$ will be a function of C_3 vs C_4 plant ratio while the vegetation composition will be determined by the hydrological conditions around a basin (δD_{water}, δD_{precip}), thus reflected in the $\delta D_{n\text{-}alkane}$. However, published phytolith data indicate that C_3 grass-dominated savanna-mosaic vegetation had become widespread in Turkey and surrounding areas by the Late Miocene (~9 Ma), while C_4 grasses were of little ecological importance in western Eurasia until at least the Late Miocene (~7 Ma) (e.g., Strömberg et al., 2007).

5.2. Alkenones and their δD and $\delta^{13}C$ isotopic compositions

Alkenones are long-chain ketones and are synthesized by unicellular eukaryotic haptophyte prymnesiophyte algae, which are common in the photic zone of the modern ocean (Volkman et al., 1980; Marlowe et al., 1984). Alkenones have been also reported from brackish and

Table 2
δD isotopes measured on alkenones from DSDP 42B 380A core. The δD of the source waters (δD_{water}) were calculated using the relations of Englebrecht and Sachs (2005) for C_{37} and C_{38} separately and Schwab and Sachs (2011) for $C_{37:2}$, $C_{37:3}$, $C_{38:2}$ and $C_{38:3}$ separately. See also the captions of Table 1.

Sample code	Depth (mbsf)	$\delta D_{C_{37}}$ (‰)	N	SEM	$\delta D_{C_{38}}$ (‰)	N	SEM	$\delta C_{C_{37}}$ (‰)	N	SEM	$\delta C_{C_{38}}$ (‰)	N	SEM	δD_w Englebrecht and Sachs (2005)		δD_w Schwab and Sachs (2011)			
														$\delta D_{C_{37}}$	$\delta D_{C_{38}}$	$\delta D_{C_{37:2}}$	$\delta D_{C_{37:3}}$	$\delta D_{C_{38:2}}$	$\delta D_{C_{38:3}}$
BS 335	933.74	−165	1		−167	1		n.d.			n.d.			82	89	15	−1	8	31
BS 333	932.70	−143	2	1.5	−147	2	1.3	n.d.			n.d.			111	115	43	36	37	56
BS 361	904.22	−176	3	0.3	−180	3	1.0	−23.8	3	0.3	−23.9	3	0.3	67	71	1	−20	−11	14
BS 364	886.63	−164	3	2.8	−168	3	1.7	−22.8	3	0.1	−22.6	3	0.2	83	87	16	0	7	29
BS 367	886.30	−147	2	0.5	−151	2	0.2	−22.8	4	0.4	−22.9	3	0.1	106	111	38	29	32	52
BS 369	884.68	−148	5	4.1	−158	5	0.6	−23.3	3	0.2	−22.8	4	0.3	105	101	37	28	21	42
BS 368	883.92	−148	6	0.6	−157	10	3.9	−24.8	1		−23.8	3	0.4	105	102	36	28	23	43
BS 401	867.62	−158	2	1.6	n.d.			−23.7	2	0.1	−24.2	2	0.3	91	n.d.	24	11	n.d.	n.d.
BS 406	867.00	n.d.			−160	2	7.6	n.d.			n.d.			n.d.	98	n.d.	n.d.	18	39
BS 408	861.40	n.d.			−164	1		−23.8	2	0.4	−23.1	2	0.7	n.d.	92	n.d.	n.d.	12	34
BS 410	858.63	−171	2	7.0	−176	2	3.7	−22.8	1		−22.1	1		74	77	8	−11	−5	19
BS 412	856.98	−178	1		−178	1	0.0	−22.8	1		−22.9	1		64	74	−1	−24	−8	16
BS 413	855.33	−224	3	1.9	−217	4		−26.8	3	0.2	−27.4	3	0.2	1	21	−59	−102	−66	−35
BS 416	850.90	−191	1		−196	2	0.8	−25.2	2	0.5	−26.4	3	0.9	46	50	−18	−46	−35	−7
BS 415	850.16	−197	4	1.9	−193	4	0.3	−25.3	2	0.6	−24.6	3	0.6	38	54	−25	−56	−29	−2
BS 417	848.50	n.d.			n.d.			−22.7	1		−27.3	1		n.d.	n.d.	n.d.	n.d.	n.d.	n.d.
BS 419	845.67	−209	2	0.7	−203	2	2.3	−25.6	3	0.0	−25.2	3	0.1	22	41	−40	−76	−44	−16
BS 422	841.26	−190	1		−172	1		−25.7	2	0.4	−25.4	2	0.4	48	82	−16	−44	1	24
BS 421	840.50	−208	2	0.2	−212	2	0.5	−27.1	2	0.1	−27.2	2	0.2	23	29	−39	−75	−57	−27
BS 424	839.80	−197	3	5.6	−194	3	2.9	−26.3	2	0.2	−25.6	2	0.2	38	52	−25	−56	−32	−5
BS 423	839.11	n.d.			n.d.			−25.2	3	0.2	−24.4	3	0.2	n.d.	n.d.	n.d.	n.d.	n.d.	n.d.
BS 426	836.86	−198	2	2.7	−194	2	0.0	−25.8	2	0.3	−25.6	2	0.3	38	52	−26	−57	−32	−4
BS 425	836.11	n.d.			n.d.			−24.6	3	0.1	−24.4	3	0.1	n.d.	n.d.	n.d.	n.d.	n.d.	n.d.
BS 428	829.20	−178	2	2.0	−157	2	0.1	−25.1	1		−25.0	1		64	101	−1	−24	22	43
BS 430	826.90	−157	1		−162	2	0.7	n.d.			n.d.			93	95	26	13	16	37
BS 434	825.80	−192	2	0.6	−170	2	2.9	−25.0	5	0.2	−24.2	5	0.2	45	85	−19	−47	4	27
BS 437	820.75	−174	3	4.2	−174	3	1.2	−26.5	1		−26.1	1		69	79	4	−17	−2	22
BS 441	809.91	n.d.			n.d.			n.d.			−24.6	1		n.d.	n.d.	n.d.	n.d.	n.d.	n.d.
BS 445	800.18	−199	2	1.4	−195	2	1.1	−24.8	2	0.2	−25.0	2	0.4	36	51	−27	−59	−34	−6
BS 447	792.10	−198	1		−183	1		−24.6	2	0.2	−24.6	2	0.0	37	68	−26	−57	−15	10
BS 451	779.65	−203	2	1.0	−194	2	1.6	n.d.			n.d.			31	52	−32	−65	−32	−5
BS 457	774.71	n.d.			n.d.			n.d.			−24.8	1		n.d.	n.d.	n.d.	n.d.	n.d.	n.d.
BS 462	757.67	n.d.			n.d.			n.d.			−23.5	3	0.3	n.d.	n.d.	n.d.	n.d.	n.d.	n.d.
BS 463	752.16	n.d.			n.d.			n.d.			−21.3	2	0.2	n.d.	n.d.	n.d.	n.d.	n.d.	n.d.

freshwater lakes from around the world (e.g., Volkman et al., 1980; Kristen et al., 2010). Changes in the relative abundance of alkenones with a different degree of unsaturation, expressed in the U^K_{37} index, are commonly used to deduce past sea surface water temperature (Brassell et al., 1986; Prahl and Wakeham, 1987).

In the Black Sea record of core 380A relative abundances of the C_{37}, C_{38} and C_{39} alkenones (Fig. 3a and d) mimics strikingly those of laboratory cultures of *Gephyrocapsa oceanica* (Sawada et al., 1996) where C_{38} alkenones overpass the contribution of C_{37} alkenones. In their research in Mutsu Bay (northern Japan), Sawada et al. (1996) observed that *G. oceanica* abundance tend to increase progressively in landward direction. Both $C_{37:2}$ and $C_{38:2}$ alkenones strongly dominate the distribution in the Black Sea core 380A. Therefore, the calculated temperatures based on the U^K_{37} proxy, would suggest very high temperatures throughout. The relative alkenone distribution does not correspond to present open marine settings, but more to coastal setting (e.g., Japan). The relative abundance of the $C_{39:2}$ alkenone in both core 380A and in the Taman section is somewhat higher than observed in open marine settings, and more similar to what has been found in the present day Black Sea and in high alkalinity lakes (Thiel et al., 1997). Whereas high alkalinity lakes show a dominant $C_{37:4}$ alkenone, this compound is absent from the Black Sea record.

The relative abundances of C_{37}, C_{38} and C_{39} are constant throughout the record (Fig. 3a and d). Because of the unknown alkenones producer(s) we refrain from calculating temperatures based on the U^K_{37} index. At Taman the $C_{37:2}$ is dominant, but still appreciable amounts of $C_{37:3}$ were detected, more in line with a haptophyte origin and relative warm but not hot temperatures.

5.2.1. Alkenone δD values

The δD composition of the alkenones reflects principally the δD of the water they live in (Englebrecht and Sachs, 2005; Schouten et al., 2005; Paul, 2002), although values are also influenced by the salinity (S_{water}), growth rate (μ_{alk}) (Schouten et al., 2005) and possibly irradiance (Pagani, 2002). $\delta D_{alkenones}$ may therefore be used as proxy to reconstruct δD_{water} (Paul, 2002; Englebrecht and Sachs, 2005; Schouten et al., 2005; Schwab and Sachs, 2011). δD measured on alkenones produced in the present day ocean range from approximately −181‰ in the warm Sargasso Sea (at 31° N) (Englebrecht and Sachs, 2005) to approximately −200‰ in temperate Chesapeake Bay (at 43° N) (Schwab and Sachs, 2011). For the modern day Black Sea the values of $\delta D_{alkenone}$ are approximately −225‰, values lighter than the rest of the ocean at the same latitude because of the influence of large amounts of fresh water input (van der Meer et al., 2008).

The results from the Hole 380 A indicate that the hydrogen isotopic composition of the C_{37} and C_{38} alkenones ($\delta D_{alkenone}$) had a variation of more than 80‰ (Table 1 and Fig. 4d). Such large offsets indicate extraordinary changes affecting the Black Sea water environment. Remarkably is that the relative abundances of C_{37}, C_{38} and C_{39} is constant throughout the record (Fig. 3a and d and Table 2), even for samples with highly contrasting $\delta D_{alkenones}$ (and $\delta^{13}C_{alkenones}$) values (Figs. 5 and 6). Based on the remarkable stability throughout the record we believe that changes in the stable isotope records do reflect actual environmental variability rather than a change in algal community composition.

The lightest values of −224‰ recorded at the 858 mbsf, in the middle of the 'aragonitic mud' (Figs. 5 and 6) are similar to the ones recorded in the Black Sea in the past 3000 years (van der Meer et al., 2008),

possibly suggesting that the connection of the Black Sea during Miocene may have been similar to present day. However, the extremely high value −143‰ for the $\delta D_{alkenone}$ observed in the Miocene deposits of units IVe, IVd and IVb indicates two phases of extreme drought. Such enriched $\delta D_{alkenone}$ has been reported previously only in the Pontian succession at Taman (Vasiliev et al., 2013). As in the case of Taman, these values hint to extraordinary conditions affecting the late Miocene Black Sea. All existing calibrations (Paul, 2002; Englebrecht and Sachs, 2005; Schouten et al., 2005; Schwab and Sachs, 2011) indicate a large variation of δD_{water}, reaching extreme positive values. Regardless of the applied relation, our $\delta D_{alkenone}$ results indicate a fast switch of the Black Sea hydrological budget (Fig. 6), with extreme evaporation prevailing during the deposition of unit IVd of 'pebbly mudstone' and top half of IVe of 'carbonates' unit. As in the case of the SST calculations from U^{K}_{37} (Prahl and Wakeham, 1987), there are limitations when applying δD_{water} reconstructions or salinity calculations based on $\delta D_{alkenone}$ because the calibration was performed on species (*Emiliania huxleyi* and *G. oceanica*) not existing in the late Miocene. Therefore only changes in absolute $\delta D_{alkenones}$ are used to infer relative changes in δD_{water}.

5.2.2. Alkenone $\delta^{13}C$ values

The $\delta^{13}C_{alkenone}$ values from the Hole 380 A are in general close to those globally recorded for marine upper Miocene (between −25‰ and −21‰) (e.g., Pagani et al., 1999) except the level with the lightest $\delta D_{alkenone}$ (−224‰) (Figs. 5 and 6). At this level, around 850 mbsf (Figs. 5 and 6), the $\delta^{13}C_{alkenone}$ values are closer to those measured for the recent Black Sea (between −26‰ and −29‰) (e.g., Freeman and Wakeham, 1992). In general, the temporal variation of $\delta^{13}C_{alkenone}$ shows a relation with the $\delta D_{alkenones}$. At 850.3 mbsf, in the middle of the 'aragonitic mud' (IVc) the lightest $\delta^{13}C_{alkenone}$ of −27.4‰, becoming some 3‰ lighter than for the older interval, and coincides with the lightest $\delta D_{alkenone}$ (−224‰). After 850.3 mbsf the $\delta^{13}C_{alkenone}$ stays for a long interval at approximately −24.8‰ (Figs. 5 and 6). Remarkably elevated $\delta D_{alkenones}$ values (at ~825 mbsf) occur at the same time as that $\delta^{13}C$ depletion in the alkenones.

5.3. SST estimates based on GDGTs

The isoprenoidal GDGT lipids, with differing numbers of pentane rings, are biosynthesized by marine *Thaumarchaeota*, occurring ubiquitously in the marine water column, while the branched GDGTs are known to be majorly produced by bacteria thriving in soils.

In our DSDP 42B 380A record, the amplitude of calculated SSTs is very large with a temperature change of 12 °C regardless of the used calibration (Fig. 6; Table 3). However, the time interval covered by our record spans millions of years, including periods of important climate changes like the Miocene–Pliocene transition. Additionally, because of the isolated character of the Black Sea the global effects may be amplified. In the DSDP 42B 380A record, below 845 mbsf (V, IVe, IVd and IVc units), the TEX_{86} estimated SSTs are just slightly higher than present day Black Sea temperatures (between 13.7 and 14.5 °C for the surface water calibration or ~8.4 °C for the calibration for 0–200 m water depth (Kim et al, 2008)). For the levels younger than 845 mbsf, corresponding to 'seekreide' (unit IVb) the TEX_{86} estimated SSTs are significantly higher than of today. Our record indicated overall increasing SSTs starting at 935 mbsf, with a superimposed large cooling event towards the top of 'aragonitic mud' IVc unit.

5.4. Paleoenvironmental reconstruction based on palynology

The combination of terrestrial (pollen and spores) and aquatic (dinoflagellate cysts, *Pediastrum* and acritarchs) palynomorphs provides an integrated tool for land–sea correlation studies of environmental changes. Dinoflagellates are single-celled, predominantly marine, eukaryotic organisms that typically occur as motile cells in surface waters. As part of their life cycle, some dinoflagellates produce resistant fossilizable cysts that can be found back in the sediments. Dinocysts have been widely used to trace past environmental changes in the

Table 3
BIT, TEX_{86} and SST estimates on DSDP 42B 380A core. The calculation of SST is based on Kim et al. (2008) calibration.

Sample code	Level (mbsf)	BIT	TEX_{86}	SST 0 m calibration	SST (0–200 m)	Sample code	Level (mbsf)	BIT	TEX_{86}	SST 0 m calibration	SST (0–200 m)
BS 462P	757.67	0.31	0.62	24.12	18.27	BS 368P	883.92	0.07	0.54	19.73	14.81
BS 462P	757.67	0.18	0.64	25.08	19.03	BS 367P	886.3	0.08	0.53	18.96	14.20
BS 457P	774.71	0.42	0.66	26.50	20.15	BS 367P	886.3	0.06	0.51	18.16	13.57
BS 451P	779.65	0.20	0.60	22.86	17.28	BS 361P	904.22	0.56	0.48	16.39	12.18
BS 447P	792.1	0.23	0.62	23.89	18.09	BS 361P	904.22	0.58	0.47	15.53	11.50
BS 445P	800.18	0.28	0.59	22.31	16.84	BS 358P	917.62	0.26	0.46	14.85	10.96
BS 444P	803.89	0.19	0.63	24.88	18.87	BS 358P	917.62	0.22	0.45	14.56	10.73
BS 441P	809.91	0.24	0.56	20.53	15.44	BS 338P	923.08	0.21	0.48	16.27	12.08
BS 437P	820.75	0.22	0.57	21.12	15.91	BS 336P	929.26	0.27	0.43	13.48	9.88
BS 435P	823.09	0.12	0.61	23.54	17.81	BS 336P	929.26	0.25	0.43	13.13	9.61
BS 436P	824.12	0.17	0.60	22.86	17.27	BS 335P	933.74	0.09	0.47	15.56	11.52
BS 434P	825.8	0.17	0.63	24.51	18.57	BS 335P	933.74	0.10	0.46	15.34	11.35
BS 429P	826.5	0.29	0.55	20.10	15.10	BS 333P	932.7	0.21	0.42	12.79	9.34
BS 431P	827.72	0.11	0.62	23.89	18.09	BS 333P	932.7	0.09	0.42	12.93	9.45
BS 427P	828.29	0.11	0.59	22.49	16.98	BS 331P	940.53	0.64	0.40	11.71	8.48
BS 426P	836.86	0.22	0.66	26.51	20.15	BS 326P	970.65	0.19	0.44	14.08	10.35
BS 424P	839.8	0.16	0.64	25.43	19.30	BS 324P	974.05	0.15	0.44	13.84	10.17
BS 422P	841.26	0.12	0.58	21.83	16.46	BS 321P	980.05	0.12	0.54	19.71	14.79
BS 421P	840.5	0.16	0.61	23.47	17.76	BS 319P	983.05	0.28	0.47	15.60	11.55
BS 419P	845.67	0.20	0.46	15.04	11.11	BS 319P	983.05	0.89	0.46	15.08	11.14
BS 417P	848.5	0.11	0.49	16.61	12.35	BS 316P	992.8	0.16	0.41	12.13	8.82
BS 416P	850.9	0.30	0.42	13.04	9.54	BS 316P	992.8	0.16	0.39	10.93	7.87
BS 415P	850.16	0.18	0.40	11.83	8.58	BS 315P	1008.13	0.27	0.46	15.13	11.18
BS 413P	855.33	0.28	0.54	19.79	14.85	BS 306P	1028.85	0.23	0.43	13.13	9.61
BS 412P	856.98	0.28	0.43	13.26	9.71	BS 305P	1027.65	0.28	0.46	14.83	10.95
BS 412P	856.98	0.27	0.41	12.52	9.12	BS 303P	1040.27	0.33	0.50	17.22	12.83
BS 410P	858.63	0.29	0.42	12.70	9.27	BS 303P	1040.27	0.33	0.50	17.49	13.04
BS 406P	867	0.22	0.46	14.81	10.93	BS 302P	1040.65	0.19	0.46	15.07	11.14
BS 406P	867	0.23	0.45	14.33	10.55	BS 302P	1040.65	0.19	0.50	17.60	13.13
BS 401P	867.62	0.46	0.52	18.67	13.97	BS 299P	1054.65	0.12	0.55	20.38	15.32
BS 369P	884.68	0.08	0.53	18.80	14.08	BS 296P	1074.34	0.11	0.39	11.11	8.01

marine realm, including the Mediterranean and Black Sea basins (e.g., Mudie et al., 2002; Sangiorgi et al., 2002, 2003; Bertini, 2006; Londeix et al., 2007, 2009; Van der Meer et al., 2008; Marret et al., 2009).

The Paratethyan endemics (*C. rugosum*, *G. etrusca* and *S. cruciformis*) and *P. psilata*, which occurs at present in the Black and Marmara seas, are associated with brackish environments (Marret et al., 2004; Bertini, 2006; Londeix et al., 2007, 2009; Zonneveld et al., 2013). The euryhaline dinocyst *L. machaerophorum* can be abundant in warm, nutrient-rich (seasonally) stratified waters influenced by river run-off (e.g., Zonneveld et al., 2013). *Spiniferites* spp. (excluding *S. cruciformis*) is a cosmopolitan genus, which thrives in a wide range of marine environments, being mainly restricted to the shelf (estuarine to neritic) environment (Brinkhuis, 1994). The green algae *Pediastrum* occurs commonly in fresh water environments (lakes or slow-moving rivers and streams), and it has also been recorded in coastal brackish waters with low salinities (<10 psu) (Bertini, 2006).

Considering the above, during the deposition of units V–IVe, Site 380 was highly influenced by terrestrial input. The high occurrence of *Pediastrum* suggests a strong influence of fresh water component in this interval, which also explains the relatively low occurrence of dinocysts and, in general, the low occurrence and/or absence of other indicators of marine conditions such as coccolithophores and foraminifers (Shipboard Scientific Party et al., 1978). The shift to marine $\delta D_{alkenone}$ values at 850.5 mbsf occurring in the aragonitic mud (IVc), is underpinned by a strong increase in the percentage of aquatic palynomorphs that persists in unit IVb. After this ingression of marine waters accompanied by a relative increase in *Spiniferites* spp., the sudden dominance of *L. machaerophorum* at ~850 m may suggest that marine waters became (seasonally) stratified due to freshwater input. Above, the sudden appearance of *P. psilata* and the Paratethyan endemics together with the presence of *L. machaerophorum* indicate a more brackish environment. This species assemblage is comparable to the present-day Caspian Sea and the early Holocene Black Sea (Marret et al., 2004, 2009) and has been interpreted as brackish lake environment with salinities between 7 and 12 psu (Mudie et al., 2002; Marret et al., 2009). The constant presence of *Pediastrum* suggests some freshwater influence, although this is significantly lower than in the part of the record predating the Pontian flooding (units V–IVe). This highlights the difference of the deposits before and after the Pontian flooding, both considered brackish water environments. The sediments after the Pontian flooding, which include *L. machaerophorum*, were likely characterized by less brackish (more saline) conditions. Little is known about the acritarch *Micrhystridium*, which has two remarkable peaks embracing the flooding event in the top of the 'pebbly mudstone' (IVd) at 867 m and in the base of the 'seekreide' (IVb) at 840 m, respectively. This species has been associated with hypersaline environments (Mudie et al., 2011), but this seems in contradiction with the marine character of the $\delta D_{alkenone}$ at ~840 m. The emergence of new habitats on the flooded continental shelf favorable for this species may explain this apparent contradiction. Alternatively, the abundance of *Micrhystridium* may represent blooms of an opportunistic acritarch species that adapted rapidly to a changing environment, especially since the 'pebbly mudstone' has been tentatively associated with a mass-wasting event from the continental shelf (Radionova and Golovina, 2011; Grothe et al., 2014). In addition, the second peak in *Micrhystridium* coincides with a major change in the water column as indicated by the switch to high SSTs, which potentially is favorable for opportunistic organisms (Fig. 6).

6. Integrated proxy data on updated age model for DSDP 42B 380A Hole

All proxy records we use in this research hint to large environmental changes, both in the Black Sea water properties and the continental realm surrounding it (Fig. 6). New dinocyst records of Grothe et al. (2014) show that the 'pebbly mudstone' (IVd) unit and the lower part of IVc, are older than the ~6.1 Ma flooding event (Chang et al., 2014) and thus considerably predate the Mediterranean MSC lowstand at 5.55 Ma and even the onset of the MSC at 5.97 Ma (Manzi et al., 2013). By far, the level with the most striking changes, clearly visible in all proxy-data, appears in the middle of the 'aragonitic mud' (IVc unit) (Figs. 5, 6 and 7) at the ~6.1 Ma flooding event (Grothe et al., 2014).

6.1. Paleoenvironmental changes in the Black Sea predating the ~6.1 Ma flooding event

The available time constraint for the lower part of the Hole 380A is provided by Kojumdgieva (1979, 1983). The author argues that unit V, and first quarter of unit IVe cover the upper part of the Volhinian and the Bessarabian (sub-stages of regional Sarmatian s.l. of Eastern Paratethys (Fig. 2)). The upper three quarters of IVe and IVd from the 380A Hole belongs to the Khersonian (Sarmatian s.l. of Eastern Paratethys (Fig. 2)). She also argues that unit IVc, comprising some marine forms of dwarfed *Bolivina* and abundant *Braarudosphaera*, belongs to the Maeotian.

Our combined proxy record for the interval before ~6.1 Ma is marked by the first occurrence of alkenones at ~935 mbsf (Fig. 6). The oldest part of the record (between ~1074 and 935 mbsf) does not contain alkenones and the estimated SST, based on TEX_{86}, fluctuates between values of 7 °C and 16 °C (Fig. 6). In this interval, terrestrial palynomorphs are very abundant, the cosmopolitan *Spiniferites* spp. is present and the freshwater *Pediastrum* becomes at times dominant; this suggests a brackish environment with relatively low salinities.

Detailed pollen analysis by Popescu (2006) indicates the presence of high amounts of thermophilous trees and very low percentages of steppe elements suggesting a warm and moist hinterland. The $\delta^{13}C_{n\text{-alkane}}$ values are fairly constant around −30‰ while the $\delta D_{n\text{-alkanes}}$ are (also rather constant) around −180‰. The corroborated proxy data hint to a relatively stable marine/brackish environment.

The level where the occurrence and/or the preservation of alkenones is observed (at ~935 mbsf, beginning of Khersonian) coincides with the moment when TEX_{86}-based SST estimates start to record a steady increase of ~6 °C until the transition between 'pebbly mudstone' and 'aragonitic mud' lithological units (Fig. 6). The $\delta D_{alkenones}$ record covering the 'carbonates', 'pebbly mudstone' and first half of the 'aragonitic mud' lithological units is strongly dominated by much enriched values when compared to the present-day marine records at this middle latitudes (Fig. 6). These heavy $\delta D_{alkenones}$ values indicate that dry conditions affected the Black Sea basin. For the same interval (with heavy $\delta D_{alkenones}$ and increasing SSTs), the palynology results indicate a strong dominance of the terrestrial palynomorphs.

The lower part of the $\delta D_{alkenone}$ record, with heavy values up to −140‰, with increasing SSTs could correspond to the Khersonian (Kojumdgieva, 1979, 1983). Accordingly, these new data indicate dry periods, with prevailing excess evaporation (Figs. 2, 4 and 5) affecting the Black Sea during the Khersonian. This interval is characterized by a significant increase in halophytes and to a lesser extent steppe, which suggests drier conditions than in the lower part of the record (Popescu, 2006). The interval between ~935 mbsf and ~855 mbsf, resembling the Khersonian and Maeotian sensu Kojumdgieva (1979, 1983), indicate dry, warm and terrestrial dominated conditions for this interval. It has been shown that, from the late Tortonian until late Messinian (from ~8 Ma to 6 Ma), the precipitation curves for the Paratethys were consistently below present-day values (Böhme et al., 2008), an observation in agreement with the spread of steppe biomes at that time in Eastern Europe (Velichko et al., 2005; Eronen, 2006). Additionally, palynofloras and macrofossil floras from south-eastern Europe and Asia Minor indicate increasingly arid-adapted dicotyledonous angiosperms by the late Miocene (e.g., Traverse, 1982; Velitzelos and Gregor, 1990; Ioakim et al., 2005). For the late Tortonian–late Messinian interval, low absolute rainfall values (~400 mm/year) were estimated for the Paratethys area (Böhme et al., 2011) while desert

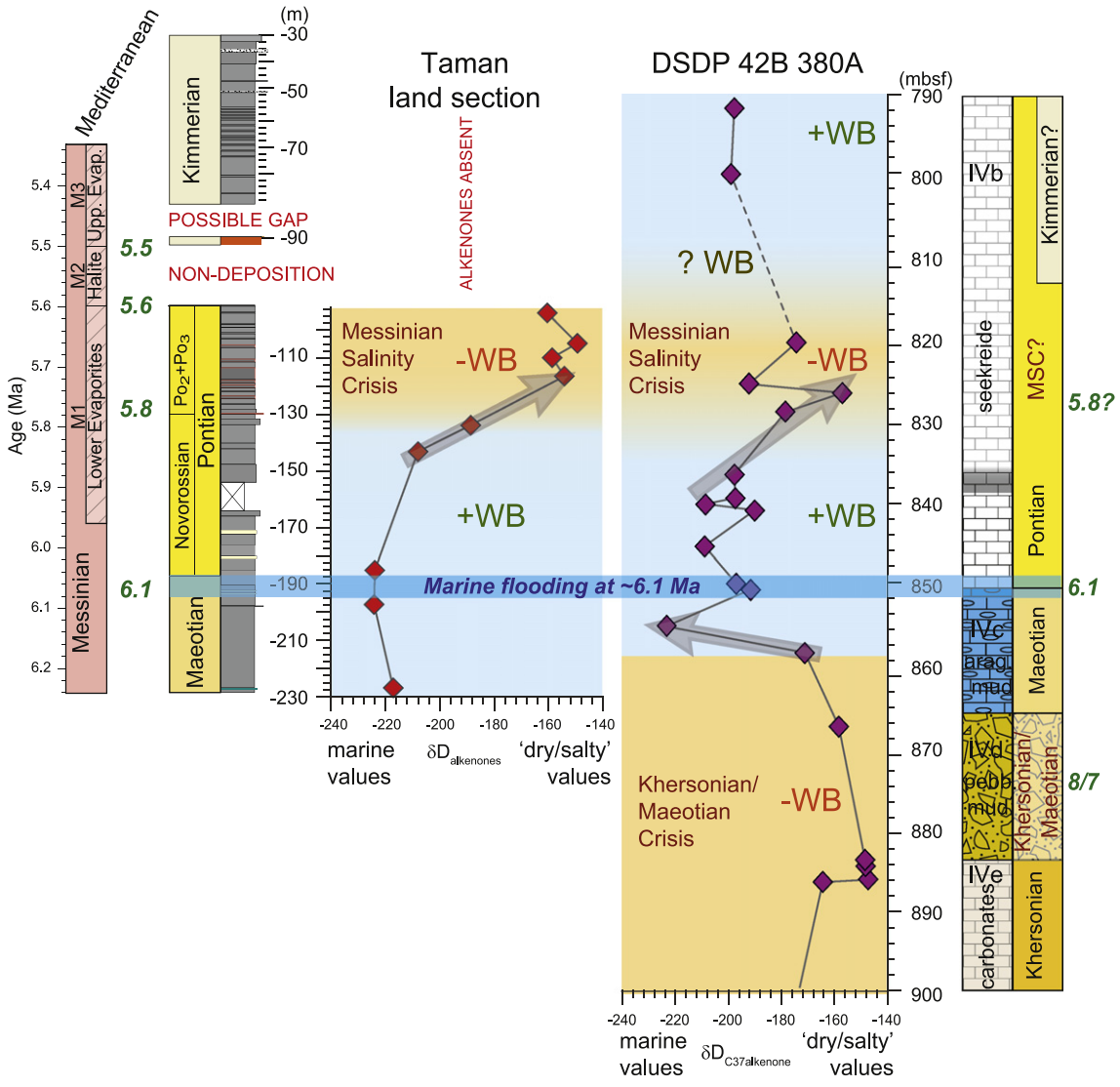

Fig. 7. Stratigraphic correlation and comparison of the $\delta D_{alkenones}$ records of DSDP Hole 380A and Zheleznyi Rog of the Taman Peninsula (modified after Vasiliev et al., 2013). The ~6.1 Ma (Krijgsman et al., 2010; Chang et al., 2014) marks the marine flooding the Paratethys at the beginning of the Pontian followed immediately by the first occurrences of *Galeacysta etrusca* and *Caspidinium rugosum* two index taxa that migrated from the Pannonian Basin into the Black Sea (Grothe et al., 2014). Green italics indicate the age in Ma. There is a 900 km distance between the location of the two sites and having different location within the Black Sea basin. The 380A hole was drilled in front of the Bosporus, at the basin slope at more than 2100 m water depth. Taman section is located on the northern coast of the Black Sea. Observe the uncertainties not fully resolved in the ages, stages and events marked by question marks. The signs of the water budget (WB) are indicated and the arrows suggest the major swishes in the hydrological budget of the Black Sea.

conditions expanded across north Africa (Zhang et al., 2014), supporting our conclusion that dry environments were characterizing the Khersonian in the Black Sea.

6.2. Paleoenvironmental changes in the Black Sea postdating the ~6.1 Ma flooding event

In the middle of the 'aragonitic mud' (IVc unit), at the ~6.1 Ma flooding event at ~855 mbsf, the $\delta D_{alkenone}$ record shows a sharp ~70‰ depletion, reaching values typical for alkenones in present day ocean waters (−220‰) (Figs. 4 and 5). This sharp switch indicates an influx of marine waters with δD values lighter than the ones existing before the deposition of unit IVc. The $\delta D_{alkenone}$ record of the Taman Peninsula shows a similar shift to light, marine-like values for the δD_{water} at the Pontian flooding (Vasiliev et al., 2013). At the same time, the $\delta^{13}C_{alkenone}$ registers ~3‰ more negative values, down to −27.4‰ (Fig. 5). These more $\delta^{13}C_{alkenone}$ depleted values coincides with TEX_{86}-based SST's estimates indicating sharp ~8 °C drop in the sea surface temperature, followed by 12 °C increase between 850 and 840 mbsf (Fig. 6). The Maeotian/Pontian transition, at ~6.1 Ma, corresponds to a relatively cold, glacial dominated global climate (Hilgen et al., 2007). Therefore, according to new data we would expect cooling taking place around this boundary. Our SSTs estimates indicate very low sea surface temperature, as low as 8 °C or 12 °C (depending on the used TEX_{86} calibration). Soon after, the SSTs indicate an increase of ~14 °C generated most probably by the influx of much warmer Mediterranean waters. A peak of *L. machaerophorum* (Fig. 6) coincides with much lighter $\delta D_{alkenone}$ and $\delta^{13}C_{alkenone}$ suggesting that the marine connection was well established at that time and density differences caused a stratified water column similar to present day (Fig. 6). The 'aragonitic mud' level is also characterized by the largest spread in the $\delta D_{n\text{-alkane}}$ values indicating either varying δD_{precip} or different (higher) plant producers of *n*-alkanes.

Another short interval with heavier $\delta D_{alkenones}$ is marked by the deposition of a peculiar extremely dark layer overlying a long light colored sequence, well visible at 826.65 mbsf (Figs. 2, 5 and 6), in

core 54 Section 1. This heavy $\delta D_{alkenones}$ event coincides with a ~8 °C cooling trend in the SSTs (Fig. 6) and corresponds to a temporary increase of the cosmopolitan *Spiniferites* spp. and relative decrease of *P. psilata*. In addition, the detailed pollen record from Popescu (2006) shows elevated abundances of herbs (e.g., *Poaceae*, *Asteraceae*, *Chenopodiaceae*), and steppe elements (*Artemisia* and *Ephedra*) at the expense of mesothermic elements (e.g., *Quercus* and *Carya*). This dark layer is thus a clear modification of the relatively stable brackish-water environment of Site 380 during the other parts of the Pontian (unit IVb).

In the outcrop section of Taman, the $\delta D_{alkenones}$ characteristic to marine water values is followed by intervals with up to −160‰ heavy $\delta D_{alkenones}$, typical for evaporative settings followed by a distinct red level, after which no alkenones are found in younger levels (Vasiliev et al., 2013; Chang et al., 2014). We speculate that the short and heavy $\delta D_{alkenones}$ event in our new 380A Hole record, marked by the dark layer at 826.65 mbsf can be correlated to the interval with heavy $\delta D_{alkenones}$ from Taman (between −120 and −90 m or ~5.8 and 5.6 Ma) (Fig. 7), thus relating to the switch in the hydrological balance observed in Taman at ~5.8 Ma (glaciations TG20 and TG22). This interval marked by the very dark layer at 826.65 mbsf, coincides with a ~8 °C cooling trend in the SSTs (Fig. 6). The thickness (i.e., duration) of this event in the Black Sea is unknown, but we can assume that deeper settings such as site 380 (Fig. 1) would have a less dramatic response in respect to the shallower settings like the one in the Taman Peninsula (Fig. 1).

7. Conclusions

Integrated analysis of organic geochemical and palynological data from the upper Miocene deposits in the DSDP Leg 42B Hole 380A show large environmental changes in the Black Sea basin and on the surrounding continental realm. Using this new proxy record superimposed on the latest age model, we propose a sequence of events archived in the succession of DSDP 42B 380A Hole from the Black Sea (Fig. 7).

1) During the deposition of unit V and the lower part of unit IVe (1072.5 mbsf to 930 mbsf — covering the upper part of the Volhinian and the Bessarabian), the Black Sea was a relatively cold sea or a lake-sea with SST decreasing to 8 °C. The absence of free alkenones in the lipid fraction could be caused either by absence of the alkenone producers or by the poor preservation of their lipids. Within the 'carbonate' of unit IVe, the sudden occurrence of the alkenones at ~930 mbsf coincides with an increasing SST trend and disappearance of *Pediastrum*. These observations, coupled with the heavy $\delta D_{alkenones}$ indicated prevailing dry conditions possibly associated with the advancement of coastal systems towards the interior of the Black Sea basin as indicated by the strong dominance of terrestrial palynomorphs. This older, longer dry/evaporative event, covering top part of IVe and entire IVd (pebbly mudstone) is older than the Maeotian/Pontian transition at ~6.1 Ma (Grothe et al., 2014). Most of the paleogeographic reconstructions indicate severe lowering of the Black Sea water level and is therefore likely associated with a regression at the end of the Khersonian. The lithological unit IVd in 380 Hole comprises stromatolitic dolomite and coarse clastic material ('pebbly mudstone' interval) that corresponds to a period of nearly complete desiccation determining what could be called the Khersonian crisis of the Black Sea (Kojumdgieva, 1979, 1983) (Fig. 7).
2) At ~858 mbsf dated now at ~6.1 Ma, the Black Sea becomes flooded by warm (Mediterranean) waters characterized by lighter $\delta D_{alkenones}$ (Fig. 7) and $\delta^{13}C_{alkenones}$. This connection is marked by the increased percentage of aquatic palynomorphs in our record and generated density and temperature driven stratification of the water column. The water stratification is well expressed as the peak appearance of *L. machaerophorum*, a dinocysts typical for stratified waters found exactly after the flooding event. The connection to the Mediterranean remains, explaining the higher SST temperatures in the Black Sea waters.
3) A short interval with heavy $\delta D_{alkenones}$ values appears at 826.65 mbsf, level coinciding with in decrease in SST. We speculate that this dry phase may be related to the switch in the hydrological balance observed in Taman at ~5.8 Ma (Fig. 7), coinciding with the TG20 and TG22 glaciations.

Supplementary data to this article can be found online at http://dx.doi.org/10.1016/j.palaeo.2015.01.020.

Acknowledgments

We are grateful to the IODP Bremen Core Repository. We thank M. Stoica and C. Van Baak for inspiring discussions on Black Sea hydrological changes, and Y.R. Mulders and T. Donders for help with palynological work. This research was financially supported by the Netherlands Earth and Life Sciences Foundation (ALW) with support from The Netherlands Organization for Scientific Research (NWO) via the Veni grant, number 863.09.006 of IV.

References

Andersen, N., Paul, H.A., Bernasconi, S.M., McKenzie, J.A., Behrens, A., Schaeffer, P., Albrecht, P., 2001. Large and rapid climate variability during the Messinian Salinity Crisis: evidence from deuterium concentrations of individual biomarkers. Geology 29, 799–802.
Bertini, A., 2006. The Northern Apennines palynological record as a contribute for the reconstruction of the Messinian palaeoenvironments. Sediment. Geol. 188, 235–258.
Böhme, M., Ilg, A., Winklhofer, M., 2008. Late Miocene "washhouse" climate in Europe. Earth Planet. Sci. Lett. 275, 393–401.
Böhme, M., Winklhofer, M., Ilg, A., 2011. Miocene precipitation in Europe: temporal trends and spatial gradients. Palaeogeogr. Palaeoclimatol. Palaeoecol. 304, 212–218.
Brassell, S.C., Eglinton, G., Marlowe, I.T., Pflaumann, U., Sarnthein, M., 1986. Molecular stratigraphy: a new tool for climatic assessment. Nature 320, 129–133.
Brinkhuis, H., 1994. Late Eocene to Early Oligocene dinoflagellate cysts from the Priabonian type-area (Northeast Italy): biostratigraphy and paleoenvironmental interpretation. Palaeogeogr. Palaeoclimatol. Palaeoecol. 107, 121–163.
Brinkhuis, H., Munsterman, D.K., Sengers, S., Sluijs, A., Warnaar, J., Williams, G.L., 2003. Late Eocene–Quaternary dinoflagellate cysts from ODP Site 1168, off western Tasmania. Proceedings of the Ocean Drilling Program, Scientific Results, Volume 189: College Station, Texas, Ocean Drilling Program, pp. 1–36.
Castañeda, I.S., Schouten, S., 2011. A review of molecular organic proxies for examining modern and ancient lacustrine environments. Quat. Sci. Rev. 30, 2851–2891.
Chang, L., Vasiliev, I., van Baak, C., Krijgsman, W., Dekkers, M.J., Roberts, A.P., van Fitz Gerald, J.D., Hoesel, A., Winklhofer, M., 2014. Identification and environmental interpretation of diagenetic and biogenic greigite in sediments: a lesson from the Messinian Black Sea. Geochem. Geophys. Geosyst. 15, 3612–3627.
Eglinton, G., Hamilton, R.J., 1967. Leaf epicular waxes. Science 156, 1322–1335.
Englebrecht, A.C., Sachs, J.P., 2005. Determination of sediment provenance at drift sites using hydrogen isotopes and unsaturation ratios in alkenones. Geochim. Cosmochim. Acta 69, 4253–4265.
Eronen, J., 2006. Eurasian Neogene large herbivore mammals and climate. Acta Zool. Fenn. 216, 1–72.
Feakins, S.J., Sessions, A.L., 2010. Controls on the D/H ratios of plant leaf waxes in an arid ecosystem. Geochim. Cosmochim. Acta 74, 2128–2141.
Feakins, S.J., Levin, N.E., Liddy, H.M., Sieracki, A.I., Eglinton, T.I., Bonnefille, R., 2013. Northeast African vegetation change over 12 m.y. Geology 41, 295–298.
Freeman, K.H., Wakeham, S.G., 1992. Variation in the distribution and isotopic composition of alkenones in Black Sea particles and sediments. Org. Geochem. 19, 277–285.
Grothe, A., Sangiorgi, F., Mulders, Y.R., Vasiliev, I., Reichart, G.J., Brinkhuis, H., Stoica, M., Krijgsman, W., 2014. Black Sea desiccation during the Messinian Salinity Crisis: fact or fiction? Geology 42, 563–566.
Hilgen, F.J., Kuiper, K.F., Krijgsman, W., Snel, E., Van der Laan, E., 2007. Astronomical tuning as the basis for high resolution chronostratigraphy: the intricate history of the Messinian Salinity Crisis. Stratigraphy 1, 231–238.
Hopmans, E.C., Schouten, S., Pancost, R.D., van der Meer, M.T.J., Sinninghe Damsté, J.S., 2000. Analysis of intact tetraether lipids in archaeal cell material and sediments by high performance liquid chromatography/atmospheric pressure chemical ionization mass spectrometry. Rapid Commun. Mass Spectrom. 14, 585–589.
Hopmans, E.C., Weijers, J.W.H., Schefuss, E., Herfort, L., Sinninghe Damsté, J.S., Schouten, S., 2004. A novel proxy for terrestrial organic matter in sediments based on branched and isoprenoid tetraether lipids. Earth Planet. Sci. Lett. 224, 107–116.
Hsü, K.J., Giovanoli, F., 1979. Messinian event in the Black Sea. Palaeogeogr. Palaeoclimatol. Palaeoecol. 29, 75–93.
Hsü, K.J., Ryan, W.B.F., Cita, M.B., 1973. Late Miocene desiccation of the Mediterranean. Nature 242, 240–244.

Huguet, C., Hopmans, E.C., Febo-Ayala, W., Thompson, D.H., Sinninghe Damsté, J.S., Schouten, S., 2006. An improved method to determine the absolute abundance of glycerol dibiphytanyl glycerol tetraether lipids. Org. Geochem. 37, 1036–1041.
IAEA, 2001. GNIP Maps and Animations. International Atomic Energy Agency, Vienna (http://isohis.iaea.org).
Ioakim, C., Rondoyanni, T., Mettos, A., 2005. The Miocene basins of Greece (Eastern Mediterranean) from a palaeoclimatic perspective. Rev. Paléobiol. 24, 735–748.
Kim, J.H., Schouten, S., Hopmans, E.C., Donner, B., Sinninghe Damste, J.S., 2008. Global sediment core-top calibration of the TEX_{86} paleothermometer in the ocean. Geochim. Cosmochim. Acta 72, 1154–1173.
Kojumdgieva, E., 1979. Critical notes on the stratigraphy of Black Sea boreholes (Deep Sea Drilling Project, Leg 42 B). Geol.Balc. 9, 107–110.
Kojumdgieva, E., 1983. Palaeogeographic environment during the desiccation of the Black Sea. Palaeogeogr. Palaeoclimatol. Palaeoecol. 43, 195–204.
Krijgsman, W., Hilgen, F.J., Raffi, I., Sierro, F.J., Wilson, D.S., 1999. Chronology, causes and progression of the Messinian Salinity Crisis. Nature 400, 652–655.
Krijgsman, W., Stoica, M., Vasiliev, I., Popov, V.V., 2010. Rise and fall of the Paratethys Sea during the Messinian Salinity Crisis. Earth Planet. Sci. Lett. 290, 183–191.
Kristen, I., Wilkes, H., Vieth, A., Zink, K.G., Plessen, B., Thorpe, J., Partridge, T.C., Oberhansli, H., 2010. Biomarker and stable carbon isotope analyses of sedimentary organic matter from Lake Tswaing: evidence for deglacial wetness and early Holocene drought from South Africa. J. Paleolimnol. 44, 143–160.
Londeix, L., Benzakour, M., Suc, J.P., Turon, J.L., 2007. Messinian palaeoenvironments and hydrology in Sicily (Italy): the dinoflagellate cyst record. Geobios 40, 233–250.
Londeix, L., Herreyre, Y., Turon, J.L., Fletcher, W., 2009. Last Glacial to Holocene hydrology of the Marmara Sea inferred from a dinoflagellate cyst record. Rev. Palaeobot. Palynol. 158, 52–71.
Manzi, V., Gennari, R., Hilgen, F., Krijgsman, W., Lugli, S., Roveri, M., Sierro, F.J., 2013. Age Refinement of the Messinian Salinity Crisis Onset in the Mediterranean Terra Nova. pp. 315–322.
Marlowe, I.T., Green, J.C., Neal, A.C., Brassell, S.C., Eglinton, G., Course, P.A., 1984. Long-chain (n-C_{37-39}) alkenones in the Prymnesiophyceae. Distribution of alkenones and other lipids and their taxonomic significance. Br. Phycol. J. 19, 203–216.
Marret, F.S. Leroy, Chalié, F., Gasse, F., 2004. New organic-walled dinoflagellate cysts from recent sediments of Central Asian seas. Rev. Palaeobot. Palynol. 129, 1–20.
Marret, F., Mudie, P., Aksu, A., Hiscott, R.N., 2009. A Holocene dinocyst record of a two-step transformation of the Neoeuxinian brackish water lake into the Black Sea. Quat. Int. 197, 72–86.
Mudie, P.J., Rochon, A., Aksu, A.E., Gillespie, H., 2002. Dinoflagellate cysts, freshwater algae and fungal spores as salinity indicators in Late Quaternary cores from Marmara and Black seas. Mar. Geol. 190, 203–231.
Mudie, P.J., Leroy, S.A.G., Marret, F., Gerasimenko, N.P., Kholeif, S.E.A., Sapelko, T., Filipova-Marinova, M., 2011. Nonpollen palynomorphs: indicators of salinity and environmental change in the Caspian–Black Sea–Mediterranean corridor. Geol. Soc. Am. Spec. Pap. 473, 89–115.
Pagani, M., 2002. The alkenone–CO_2 proxy and ancient atmospheric carbon dioxide. Philos. Trans. R. Soc. Lond. 360, 609–632.
Pagani, M., Freeman, K.H., Arthur, M.A., 1999. Late Miocene atmospheric CO_2 concentrations and the expansion of C_4 gasses. Science 285, 876–879.
Pagani, M., et al., 2006. Arctic hydrology during global warming at the Palaeocene/Eocene thermal maximum. Nature 442, 671–675.
Paul, H.A., 2002. Application of Novel Stable Isotope Methods to Reconstruct Paleoenvironments: Compound-specific Hydrogen Isotopes and Pore-water Oxygen Isotopes. (Ph. D. Thesis), Swiss Federal Institute of Technology, Zurich (141 pp.).
Polissar, P.J., Freeman, K.H., 2010. Effects of aridity and vegetation on plant-wax δD in modern lake sediments. Geochim. Cosmochim. Acta 74, 5785–5797.
Popescu, S.M., 2006. Late Miocene and early Pliocene environments in the southwestern Black Sea region from high-resolution palynology of DSDP Site 380A (Leg 42B). Palaeogeogr. Palaeoclimatol. Palaeoecol. 238, 64–77.
Prahl, F.G., Wakeham, S.G., 1987. Calibration of unsaturation patterns in long-chain ketone compositions for paleotemperature assessment. Nature 330, 367–369.
Radionova, E.P., Golovina, L.A., 2011. Presumably Messinian deposits in the Black Sea (Sites 380A, 381 DSDP and Zheleznyi Rog section of Taman Peninsula). In: Sierro, F.J., Gonzalez-Delgádo, J.A. (Eds.), Climate Changes, Bio-events and Geochronology in the Atlantic and Mediterranean Over the Last 23 Myr: Joint Regional Committee on Mediterranean Neogene Stratigraphy (RCMNS)–Regional Committee on Atlantic Neogene Stratigraphy (RCANS). Interim Colloquium, Salamanca, Spain, pp. 21–23 (September 2011, Abstracts Book, p. 201).
Rögl, F., 1999. Mediterranean and Paratethys. Facts and hypotheses of an Oligocene to Miocene paleogeography (short overview). Geol. Carpath. 50, 339–349.
Ross, D.A., Neprochnov, Y.P., 1978. Initial Reports of the Deep Sea Drilling Project, Volume 42, Part 2. U.S. Government Printing Office, Washington.
Roveri, M., Flecker, R., Krijgsman, W., Lofi, J., Lugli, S., Manzi, V., Sierro, F.J., Bertini, A., Camerlenghi, A., De Lange, G., Govers, R., Hilgen, F.J., Hübscher, C., Meijer, P.T., Stoica, M., 2014. The Messinian Salinity Crisis: past and future of a great challenge for marine sciences. Mar. Geol. 352, 25–58.
Sachse, D., Radke, J., Gaupp, R., Schwark, L., Lüniger, G., Gleixner, G., 2004a. Reconstruction of palaeohydrological conditions in a lagoon during the 2nd Zechstein cycle through simultaneous use of δD values of individual *n*-alkanes and $\delta^{18}O$ and $\delta^{13}C$ values of carbonates. Int. J. Earth Sci. 93, 554–564.
Sachse, D., Radke, J., Gleixner, G., 2004b. Hydrogen isotope ratio of recent lacustrine sedimentary n-alkanes record modern climate variability. Geochim. Cosmochim. Acta 68, 4877–4889.
Sachse, D., Radke, J., Gleixner, G., 2006. δD values of individual *n*-alkanes from terrestrial plants along a climatic gradient — implications for the sedimentary biomarker record. Org. Geochem. 37, 469–483.
Sangiorgi, F., Capotondi, L., Brinkhuis, H., 2002. A centennial scale organic-walled dinoflagellate cyst record of the last deglaciation in the South Adriatic Sea (Central Mediterranean). Palaeogeogr. Palaeoclimatol. Palaeoecol. 186, 199–216.
Sangiorgi, F., Capotondi, L., Combourieu Nebout, N., Vigliotti, L., Brinkhuis, H., Giunta, S., Reichart, G.J., 2003. Holocene seasonal sea-surface temperature variations in the southern Adriatic Sea inferred from a multiproxy approach. J. Quat. Sci. 18, 723–732.
Sawada, K., Handa, N., Shiraiwa, Y., Danbara, A., Montani, S., 1996. Long-chain alkenones and alkyl alkenoates in the coastal and pelagic sediments of the northwest North Pacific, with special reference to the reconstruction of *Emiliania huxleyi* and *Gephyrocapsa oceanica* ratios. Org. Geochem. 24, 751–764.
Schefuss, E., Schouten, S., Schneider, R.R., 2005. Climatic controls on central African hydrology during the past 20,000 years. Nature 437, 1003–1006.
Schouten, S., Hopmans, E.C., Schefuss, E., Sinninghe Damsté, J.S., 2002. Distributional variations in marine crenarchaeotal membrane lipids: a new tool for reconstructing ancient sea water temperatures? Earth Planet. Sci. Lett. 204, 265–274.
Schouten, S., Ossebaar, J., Schreiber, K., Kienhuis, M.V.M., Langer, G., Bijma, J., 2005. The effect of temperature and salinity on the stable hydrogen isotopic composition of long chain alkenones produced by *Emiliania huxleyi* and *Gephyrocapsa oceanica*. Biogeosci. Discuss. 2, 1681–1695.
Schwab, V., Sachs, J.P., 2011. Hydrogen isotopes in individual alkenones from the Chesapeake Bay estuary. Geochim. Cosmochim. Acta 75, 7552–7565.
Shipboard Scientific Party, 1978. In: Ross, D.A., Neprochnov, Y.P., et al. (Eds.), Initial Reports of the Deep Sea Drilling Project, Volume 42, Part 2. U.S. Government Printing Office, Washington, pp. 483–488.
Sessions, A.L., Burgoyne, T.W., Schimmelmann, A., Hayes, J.M., 1999. Fractionation of hydrogen isotopes in lipid biosynthesis. Org. Geochem. 30, 1193–1200.
Speelman, E.N., Sewall, J.O., Noone, D., Huber, M., von der Heydt, A., Sinninghe Damsté, J., Reichart, G.J., 2010. Modeling the influence of a reduced equator-to-pole sea surface temperature gradient on the distribution of water isotopes in the Early/Middle Eocene. Earth Planet. Sci. Lett. 298, 57–65.
Strömberg, C.A.E., Werdelin, E., Friis, E.M., Saraç, G., 2007. The spread of grass-dominated habitats in Turkey and surrounding areas during the Cenozoic: phytolith evidence. Palaeogeogr. Palaeoclimatol. Palaeoecol. 250, 18–49.
Thiel, V., Jenisch, A., Landmann, G., Reimer, A., Michaelis, W., 1997. Unusual distributions of long-chain alkenones and tetrahymenol from the highly alkaline Lake Van, Turkey. Geochim. Cosmochim. Acta 61, 2053–2064.
Tipple, B.J., Pagani, M., 2010. A 35 Myr North American leaf-wax compound-specific carbon and hydrogen isotope record: implications for C_4 grasslands and hydrologic cycle dynamics. Earth Planet. Sci. Lett. 299, 250–262.
Traverse, A., 1982. Response of world vegetation to Neogene tectonic and climatic events. Alcheringa 6, 197–209.
van der Meer, M.T.J., Sangiorgi, F., Baas, M., Brinkhuis, H., Sinninghe Damsté, J.S., Schouten, S., 2008. Molecular isotopic and dinoflagellate evidence for Late Holocene freshening of the Black Sea. Earth Planet. Sci. Lett. 267, 426–434.
Vasiliev, I., Iosifidi, A.G., Khramov, A.N., Krijgsman, W., Kuiper, K.F., Langereis, C.G., Popov, V.V., Stoica, M., Tomsha, V.A., Yudin, S.V., 2011. Magnetostratigraphy and radiometric dating of upper Miocene–lower Pliocene sedimentary successions of the Black Sea basin (Taman Peninsula, Russia). Palaeogeogr. Palaeoclimatol. Palaeoecol. 310, 163–175.
Vasiliev, I., Reichart, G.J., Krijgsman, W., 2013. Impact of the Messinian Salinity Crisis on Black Sea hydrology — insights from hydrogen isotopes on molecular biomarkers. Earth Planet. Sci. Lett. 362, 272–282.
Velichko, A.A., Akhlestina, E.F., Borisowa, O.K., Gribchnko, Y.N., Zhidovinov, N.Y., elikson, E.N., Iosifova, Y.I., Klimanov, V.A., Morosova, T.D., Nechaev, V.P., Pisareva, V.V., Svetlitskaya, T.V., Spasskaya, I.I., Udartsev, V.P., Faustova, M.A., Shik, S.M., 2005. East European plain. In: Velichko, A.A., Nechaev, V.P. (Eds.), Cenozoic Climatic and Environmental Changes in Russia. Geological Society of America, pp. 31–66.
Velitzelos, E., Gregor, H.-J., 1990. Some aspects of the Neogene floral history in Greece. Rev. Palaeobot. Palynol. 62, 291–307.
Volkman, J.K., Eglinton, G., Corner, E.D.S., Forsberg, T.E.V., 1980. Long chain alkenes and alkenones in the marine coccolithophorid *Emiliania huxleyi*. Phytochemistry 19, 2619–2622.
Weijers, J.W.H., Schouten, S., Spaargaren, O.C., Sinninghe Damsté, J.S., 2006. Occurrence and distribution of tetraether membrane lipids in soils: implications for the use of the TEX_{86} proxy and the BIT index. Org. Geochem. 37, 1680–1693.
Zhang, Z., Ramstein, G., Schuster, M., Li, C., Contoux, C., Yan, Q., 2014. Aridification of the Sahara Desert caused by Tethys Sea shrinkage during the Late Miocene. Nature 513, 401–404.
Zonneveld, K.A., Marret, F., Versteegh, G.J., Bogus, K., Bonnet, S., Bouimetarhan, I., Young, M., 2013. Atlas of modern dinoflagellate cyst distribution based on 2405 data points. Rev. Palaeobot. Palynol. 191, 1–197.